



UNIVERSIDAD DE LA LAGUNA
INSTITUTO DE ASTROFÍSICA DE CANARIAS

Trabajo de Fin de Máster

Cosmological observations with virtual radio telescopes

Autora:

Ángela María Arriero López

Supervisor:

Michael Peel

Trabajo presentado en cumplimiento de los requisitos para optar al grado de:

Máster en Astrofísica

30/06/2022

Abstract

The ground-based radio telescopes simulation software enable us to optimise the configuration of the telescope and its instrument dedicated to the observation of the Cosmic Microwave Background (CMB). This type of observations requires very high sensitivity in data acquisition; therefore, designing a code that allows changing the properties of the telescope to obtain simulated CMB maps is of great importance.

Thus, the simulation of the GroundBIRD radio telescope currently located at the Teide Observatory in Spain was developed. For this, we used the classes and functions provided by the TOAST framework, a software developed in Python that supports telescope projects dedicated to observing the CMB, such as Planck and LiteBIRD (space telescopes), and ground-based projects such as the Simons Array and CMB-S4. This work provides an adapted functional code made in Python that simulates the main features of the GroundBIRD telescope and generates intensity and polarization (Q-U) CMB maps from the Map-Making process developed by the TOAST framework, which uses the library Libmadam to remove correlated noise.

Furthermore, the project shows the behavior of the polarization signals in EE and BB mode before based on varying characteristics such as the integration time of the observations, the polarization angles of the focal plane detectors, the Noise Equivalent Temperature (NET) of the detectors, the knee frequency of the $1/f$ noise and the elevation and scan speed of the telescope. It was observed that the noise level of the maps decreases significantly when: the integration time is longer; there are four rather than two polarization detector angles; the Noise Equivalent Temperature (NET) is reduced to $2.5 \mu K \sqrt{s}$, and when the telescope elevation is 60° . It was also found that the power spectrum of the output CMB signal is similar to the input CMB when the knee frequency of the $1/f$ noise is less than 1 Hz and when the scan speed is 20 rpm.

To conclude, we can say that the current features of GroundBIRD, based on the performed simulations, allow measuring low power signals at low multipoles with relatively low noise levels. However, the simulation could be improved to take into account real $1/f$ noise levels, background effects due to polarization generated by thermal or synchrotron radiation, atmospheric noise, and ground signals.

Resumen

El software de simulación de radiotelescopios terrestres permite optimizar la configuración del telescopio y sus instrumentos dedicados a la observación del Fondo Cósmico de Microondas (CMB, por sus siglas en inglés). Este tipo de observaciones requiere una sensibilidad muy alta en la adquisición de datos, por lo que diseñar un código que permita cambiar las propiedades del telescopio para obtener mapas simulados del CMB es de gran importancia.

Así, se desarrolló la simulación del radiotelescopio GroundBIRD actualmente ubicado en el Observatorio del Teide en España. Para ello, se utilizaron las clases y funciones proporcionadas por el framework TOAST, un software desarrollado en Python que da soporte a proyectos de telescopios dedicados a la observación del CMB, como Planck y LiteBIRD (telescopios espaciales), y a proyectos en tierra como el Simons Array y el CMB-S4. Este trabajo proporciona un código funcional adaptado realizado en Python que simula las principales características del telescopio GroundBIRD y genera mapas de intensidad y polarización (Q-U) del CMB a partir del proceso de Map-Making desarrollado por el framework TOAST, que utiliza la librería Libmadam para eliminar el ruido correlacionado.

Además, el proyecto muestra el comportamiento de las señales de polarización en modo EE y BB antes en función de la variación de características como el tiempo de integración de las observaciones, los ángulos de polarización de los detectores del plano focal, la Temperatura de Ruido Equivalente (NET por sus siglas en inglés) de los detectores, la frecuencia de rodilla del ruido $1/f$ y la elevación y velocidad de escaneo del telescopio. Se observó que el nivel de ruido de los mapas disminuye significativamente cuando: el tiempo de integración es mayor; hay cuatro en lugar de dos ángulos de polarización de los detectores; la Temperatura de Ruido Equivalente (NET) se reduce a $2.5 \mu K \sqrt{s}$, y cuando la elevación del telescopio es de 60° . También se encontró que el espectro de potencia de la señal CMB de salida es similar al CMB de entrada cuando la frecuencia de rodilla del ruido $1/f$ es inferior a 1 Hz y cuando la velocidad de escaneo es de 20 rpm.

Para concluir, podemos decir que las características actuales de GroundBIRD, basadas en las simulaciones realizadas, permiten medir señales de baja potencia en multipolos bajos con niveles de ruido relativamente bajos. Sin embargo, la simulación podría mejorarse para tener en cuenta los niveles reales de ruido $1/f$, los efectos de fondo debidos a la polarización generada por la radiación térmica o sincrotrón, el ruido atmosférico y las señales de tierra.

Contents

Abstract	i
Resumen	ii
1. Introduction	1
1.1. Scientific Background	1
1.1.1. Cosmic Microwave Background (CMB)	2
1.1.2. CMB anisotropies	3
1.1.3. Power spectrum	4
1.1.4. Polarization: E-B modes	4
1.2. Telescope and Simulations	6
1.2.1. GroundBIRD Telescope	6
1.2.2. Simulations: TOAST framework	9
1.3. Objectives	11
2. Methodology	12
2.1. Simulation computational resources	12
2.2. Code development	12
2.2.1. Module A: Time Ordered Distribution object	14
2.2.2. Module B: DistPixel Function	20
2.2.3. Module C: Sky signal and Full signal	21
2.2.4. Module D:Map-making	21
3. Results and Discussion	23
3.1. Virtual Radio Telescope	23
3.2. Integration Time	25
3.3. Focal Plane	28
3.4. NET	30
3.5. Knee Frequency	32
3.6. Elevation	34
3.7. Scan Rate Velocity	36
4. Conclusions	38
A. Appendix	41
A.1. Simulations: <i>TOAST Classes</i>	41
A.2. Module B	43

Contents

A.3. Module C	43
List of Figures	45
List of Tables	48
Bibliography	49

1. Introduction

1.1. Scientific Background

The Big Bang theory describes well the observable cosmological data collected today. The Universe was created 14 billion years ago in a great explosion called the Big Bang (Carroll et al., 2014; Schneider, 2015). After this explosion, the Universe was filled with a very hot and dense plasma of particles (electrons, protons and neutrons) and radiation (photons), which rapidly expanded through space due to the *Inflation*. Due to this expansion, the radiation cooled to become the Cosmic Microwave Background (CMB) which will be the faint remnant of this primordial radiation (Perlov et al., 2017). The CMB was discovered in 1965 by Arno Penzias and Robert Wilson when testing a sensitive radio antenna for Bell Telephone Laboratories in New Jersey (Carroll et al., 2014; Penzias et al., 1965).

The Cosmic Microwave Background (CMB) is an isotropic blackbody radiation originated when the Universe was about 3.8×10^5 years old ¹. This electromagnetic radiation is explained under the Big Bang theory, which proposes an evolution of the Universe from a very dense and hot state that cooled over time (Carroll et al., 2014). The CMB temperature is about 2.725 K and is brightest at microwave frequencies. The Big Bang theory cannot explain the isotropic behavior of the CMB by itself (Perlov et al., 2017). In 1980 a group of cosmologist proposed a possible solution in which a rapid and exponential expansion of the Universe called *Inflation* would have been generated after the Big Bang.

This model predicts that the CMB contains some anisotropies in its intensity and polarization that allow determining parameters of the standard cosmological model (Carroll et al., 2014; Perlov et al., 2017; KRAGH, 2007; Peacock, 2010). To observe such anisotropies, some experiments have been developed both on the ground and in space that have achieved great precision in the measurements of the maps obtained by observations. The first satellite launched by an USSR satellite to measure the CMB dipole was RELIKT-1 in 1983. Then, a second satellite called COsmic Background Explorer (COBE) was launched in 1989 by NASA.

COBE satellite proved, for the first time, the existence of expected anisotropies in temperature maps; measuring quite accurately the CMB temperature of 2.725 K (Perlov et al., 2017). Subsequently, satellites such as *Wilkinson Microwave Anisotropy Probe* or WMAP (NASA) and the DASI ground experiment (Degree Angular Scale Interferometer) successfully observed

¹https://www.esa.int/Science_Exploration/Space_Science/Planck/Planck_and_the_cosmic_microwave_background

the angular temperature Power Spectrum and the polarization E-mode respectively, in 2003. Finally the Planck satellite made very-high-resolution maps of the CMB between 2009 and 2013 ²³ (Ade et al., 2016).

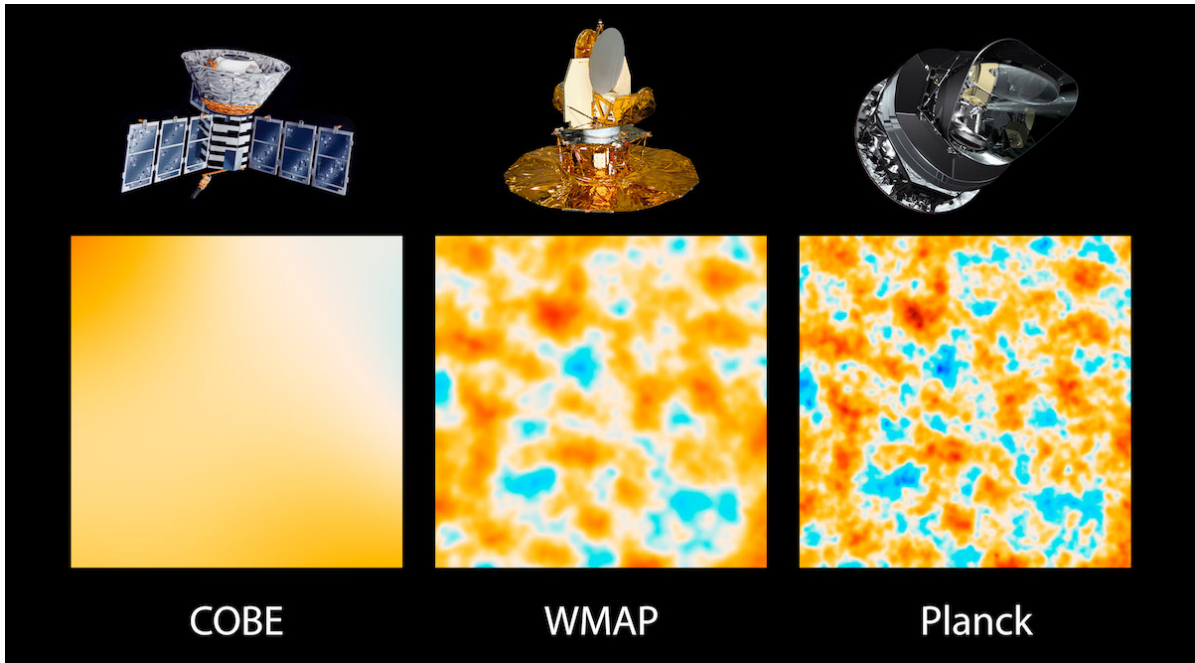


Figure 1.1.: The three panels show 10-square-degree patches of all-sky maps. Image credit: NASA/JPL-Caltech/ESA

1.1.1. Cosmic Microwave Background (CMB)

The study of the CMB radiation has generated constraints in understanding the evolution of the universe for years. Although the Big Bang has been a very successful theory because it predicts the primordial nuclear abundances, the properties of the Microwave Background Radiation, and explains how the formation of galaxies and clusters occurred, the theory has some problems in explaining the geometry of the Universe, the homogeneity on large scales, the origin of small density fluctuations, and the expanding Universe (Carroll et al., 2014).

The Big Bang postulates that the Universe had a homogeneous expansion and was nearly flat at the beginning (Perlov et al., 2017). Due to the CMB uniformity in its temperature across the sky, it indicates that the universe was fairly homogeneous when the radiation was emitted, resulting in what is know as the *Horizon Problem*. The problem is that information cannot travel faster than the speed of light, so two regions of the space separated by a distance greater that light can travel cannot be causally connected; therefore, the isotropy observed in

²https://www.esa.int/Enabling_Support/Operations/Planck

³https://www.nasa.gov/mission_pages/planck/multimedia/pia16874.html

the CMB represents a challenge to explain (Peacock, 2010).

In 1981 a possible solution was proposed: after the Big Bang there would have been a rapid and exponential expansion of the Universe called *Inflation*. After Inflation, light and matter were created. Matter was colliding frequently, meaning photons could not travel long distances, so the Universe was opaque in early states. As was mentioned, the Universe were cooling down due to expansion, and when temperature was low enough around 3000 K, the particles collided less, allowing electrons and protons to combine, creating Hydrogen atoms. This era is known as *recombination* (Ransom, 2016)⁴.

When the era of recombination ended, the temperature was getting lower and the electrons could not escape from the protons, so the density of free electrons started to decrease and the photons were able to move unhindered through the Universe. As a result, a geometrical place was created where this background radiation had the last interaction before definitely decoupling, what is named "the surface of the last scattering".

This surface of last scattering defines the limit of the visible Universe, and it represents the maximum redshift in which the Universe is observable through photons (Ransom, 2016; Cepa, 2007). The scattering process is a statistical process, i.e., anisotropy photons would not be decoupling all at the same time, so this last scattering surface will have a finite thickness (Cepa, 2007). These photons have been changing their wavelength due to the expansion of the Universe and today reach us as microwave radiation. Since photons no longer interact with matter, the blackbody distribution imprinted by the CMB remains. However, there are some processes that would affect the photons coming from the background radiation, changing the blackbody spectrum or generating anisotropies (Cepa, 2007).

1.1.2. CMB anisotropies

Due to the existence of structures such as stars and galaxies, density inhomogeneities owing to gravity instabilities should exist on large or small scales. Anisotropies in the angular distribution of the CMB temperature are variations in matter due to density fluctuations in the recombination epoch. These can be classified by angular scale (large scale $\ell < 200$, intermediate scale $200 < \ell < 1000$, and small scale $\ell > 1000$). Also as primary anisotropies (generated on the last scattering surface), and secondary anisotropies (generated on the path from the last scattering surface to now, e.g., galaxy clusters, super galaxy clusters (Cepa, 2007)), and also, as mathematical terms: scalar (fluctuations in density and pressure), vectorial (velocity), and tensorial (gravitational waves) (Cepa, 2007).

The mechanisms responsible for generating anisotropies are density variations, the Sachs-Wolfe effect (gravitational potential effects) and the Doppler effect (the increase in density causes the movement of the material when it interacts with gravity) (Cepa, 2007). Primary

⁴https://www.esa.int/Science_Exploration/Space_Science/Planck/Planck_and_the_cosmic_microwave_background

anisotropies result from gravitational redshift at large angular scales, the evolution of the primordial photon-baryon fluid due to gravity, and the Compton scattering at lower scales (Aghanim et al., 2008). Furthermore, the anisotropies in which photons reach us and interact with cosmic structures and their properties such as frequency, energy, or change in direction of propagation are called "secondary anisotropies" (Aghanim et al., 2008).

Secondary anisotropies could be divided into two large families. The first one includes anisotropies generated by the interaction of the photons with gravitational potential wells (gravitational lensing, Reiss-Sciama effect RS, and the integrated Sachs-Wolfe effect ISW), and the second one is related to scattering effects between CMB photons and free electrons (Compton interaction: the Sunyaev-Zel'dovich SZ), velocity-induced scatterings (Ostriker-Vishniac OV) and inhomogeneous reionization) (Aghanim et al., 2008).

1.1.3. Power spectrum

Density fluctuations can be described by the statistical properties of the mass distribution. There are a large number of statistical properties for the density field that can be quantitatively explained if we have the correct model of cosmological structure formation. This statistical description in cosmology is done by the correlation function that characterizes the structure of the cosmological distribution of matter and the power spectrum $P(k)$ which statistically describes the properties of a random field (distribution of matter in a Universe), and is defined as the Fourier transform of the correlation function.

Nevertheless, this exact definition cannot be applied to the CMB since the density fluctuations are defined over a flat space, and in our case the temperature fluctuations are defined over a sphere, for this, the analog to the Fourier modes in the sphere is the spherical harmonics that at small angular scales the sphere is considered locally flat, and the harmonics behave like plane waves. The power spectrum of temperature fluctuations describes the amplitude of the fluctuation as $\ell(\ell + 1)C_\ell$ in terms of the angular scale $\theta \sim \pi/\ell$ (Schneider, 2015) as shown in figure 1.3 (b).

1.1.4. Polarization: E-B modes

The inflation theory predicts that primordial gravitational waves would have been created, and would have left their imprint on the polarization information of the photons that might pass through the surface of the last (Choi, 2015) scattering. These primordial gravitational waves were formed before the surface of the last scattering and are the earliest signal we can see in our Universe. These gravitational waves were generated by quantum fluctuations in the geometry of space-time. Their wavelengths were extended to astronomical sizes due to inflationary expansion and propagated throughout the Universe, and the effects of these waves on the CMB radiation impacted temperature fluctuations and would have caused (Perlov et al., 2017) polarization patterns.

The polarization in the CMB is due to Thomson scattering of radiation with a *quadrupole* anisotropy and a free electron in the photon-baryon fluid. As a result, it generates a linear polarization as shown in figure 1.2 (a). Polarization is generated when the photon electric field is oriented in a certain way. Gravitational waves pass through plasma (Photon-Baryon fluid) on recombination, and there are two ways of produce a local *quadrupole* moment in the CMB. One by the flow of the photon-baryon fluid and two by the effect of gravitational radiation (Carroll et al., 2014; Hu, 2003; Hu et al., 1997).

When a gravitational wave passes through the photon-baryon fluid, the space containing the photons is stretched along one axis while it is compressed along a perpendicular axis, producing a quadrupole moment in the radiation field (Carroll et al., 2014; Hu et al., 1997).

Furthermore, the polarization of the CMB radiation presents two polarization modes regarding to its orientation, E and B modes. These modes at small scales are simply to visualize. The E-mode which is generated by primordial density fluctuations (radial and ring-like structures) and B-modes due to gravitational waves (show like swirl-like pattern) as figure 1.2 (b) shows (Carroll et al., 2014; Perlov et al., 2017).

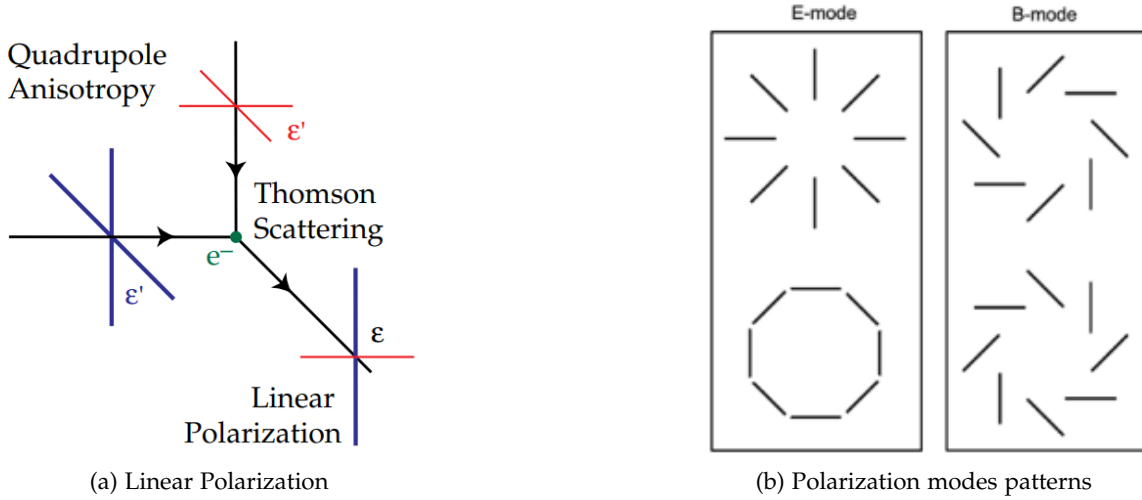


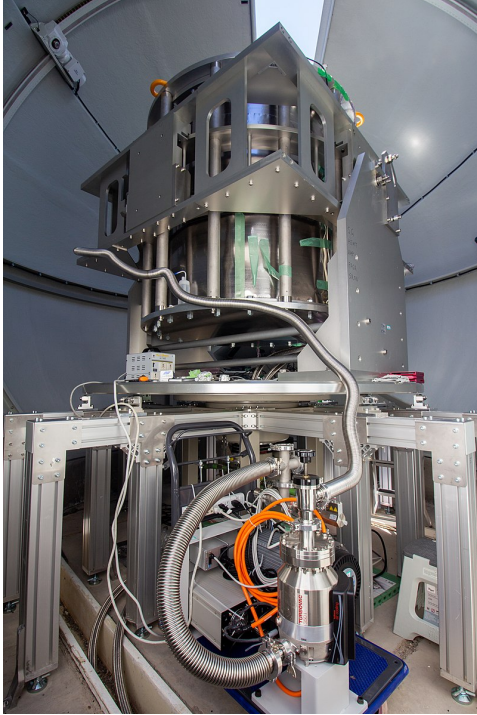
Figure 1.2.: Figure (a) shows the Thomson scattering effect when radiation an a quadrupole anisotropy generates linear polarization taken from (Hu et al., 1997). Figure (b) shows the polarization modes patterns generated by anisotropies taken from (Perlov et al., 2017)

No evidence has been found to date for the primordial B-modes, which are expected to be measured for $\ell < 100$ and which could reveal information about the physics of the early Universe (when and how inflation occurred). However, B-modes coming from gravitational lensing have been detected by POLARBEAR, SPT and BICEP as figure 1.3 (b) shows. The B-modes are represented by the parameter called the tensor-to-scalar ratio r and its upper limit is currently at $r < 0.036$ measured by the combination of the ground-based BICEP

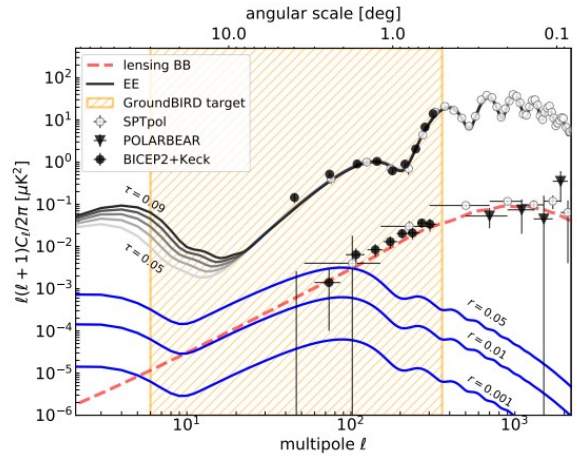
experiments and the Planck Space Telescope (Ade et al., 2021).

1.2. Telescope and Simulations

1.2.1. GroundBIRD Telescope



(a) GroundBIRD Telescope



(b) Polarization Power Spectrum

Figure 1.3.: Figure (a) shows GroundBIRD telescope in the Teide observatory. Tenerife, Spain. Figure (b) shows the polarization Power Spectrum (PS) of the anisotropies as a function of the multipole. The orange region shows the GroundBIRD observation region Kutsuma, 2021

GroundBIRD is a ground-based experiment and its objective is to study the large angular scale of the primordial polarization B-modes imprinted in the Cosmic Microwave Background, and which so far have not been measured. The telescope shown in figure 1.3 (a) ⁵ is located at the Teide Observatory, and its main specifications are shown in table 1.1. The experiment began test operations in September 2019 (Honda et al., 2020), and the organizations participating in the project are: RIKEN (Japan Institute of Natural Sciences), Kyoto University, Tohoku University, KEK, NAOJ, Tohoku University, Tokyo University, Saitama University, Korea University, KASI, SRON and the IAC.

This B-mode pattern will provide important evidence of cosmological inflation and will be measured by GroundBIRD in the multipole range between $6 < \ell < 300$ with a sensitivity

⁵<https://en.wikipedia.org/wiki/GroundBIRD>

of tensor-to-scalar ratio $r = 0.01$ (see figure 1.3 (b)) for three years of observation (Choi, 2015; Kutsuma, 2021) .

To get this objective, the telescope has three main features which will guarantee will help it to achieve the fulfillment of said goal(Choi, 2015; Lee, K. et al., 2020):

- **Fast rotational scanning:** This experiment is able to address the primordial B-mode reionization bump from the ground mitigating the atmospheric $1/f$ fluctuation. The experiment performs fast rotation scans around the zenith direction with a telescope tilt of 30° from zenith at a rate of 20 rotations per minute, whereby the sky area coverage due to the earth rotation will be 50% in a day, which is more than the capacity of observations of the current ground-based telescopes.
- **Cooling of the optical system:** Since the high rotation speed is necessary to avoid the $1/f$ atmospheric noise, the cooling system should be avoid thermal noise which could damage the focal plane and optics performance.
- **Super-conducting focal plane detector MKID:** The fast rotation scanning and the weakness of the B-mode signal means that the telescope requires detectors in the focal plane with high accuracy and fast read time. KID is a kinetic inductance detector which has a superconductor circuit that accelerates and decelerates electrons. Its kinetic inductance increases as the density of Cooper electron pairs decreases. A photon which interacts with the superconductor will disrupt one or more Cooper pairs, decreasing their density and increasing the kinetic inductance. Combining this device with a capacitor, a resonant circuit is formed whose frequency is in the microwave region or a MKID device. The MKID has a time response $< 100 \mu s$ and has the ability to read about 1000 pixels for a single line out (Kitchin, 2013).

Aperture diameter	300 mm
Optics	Cross Dragone, FOV = $\pm 10^\circ$
Observation frequency	145 and 220 GHz
Resolution	0.5° at 145 GHz, 0.3° at 220 GHz
Scan speed	$120^\circ / s$
Coverage	30 % of the full sky 12,000 deg ²

Table 1.1.: GroundBIRD telescope principal specifications taken from Choi, 2015

Regarding the focal plane, the observation frequencies are 145 and 220 GHz. At the 145 GHz frequency it is possible to observe the CMB polarization, this is because at this frequency this polarization is relatively stronger than the polarization generated by the dust and synchrotron emissions; while at the 220 GHz frequency, we can measure the thermal radiation emitted by the dust (see figure 1.5) which must be removed at the end of the observations, and subsequently can be used for measurements performed by other previous experiments (Lee

et al., 2021).

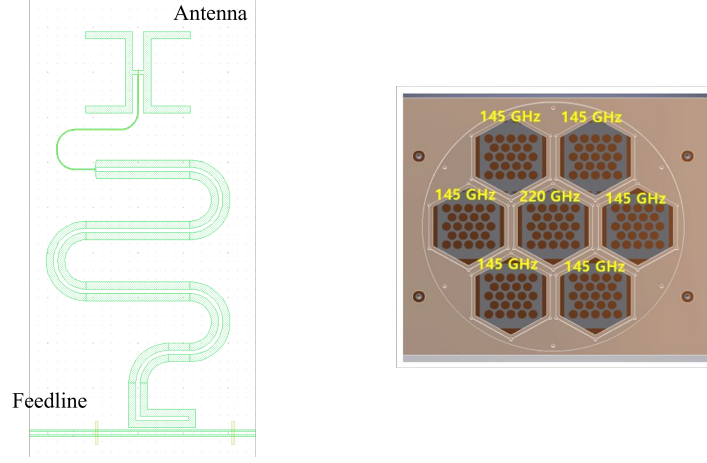


Figure 1.4.: Left: the electronic design of each pixel in the focal plane. Right: shows the layout of the focal plane. It contains 7 modules and 23 pixels for each module (Lee et al., 2020)

The focal plane has 7 hexagonal shaped modules shown in figure 1.4. The central module measures radiation at 220 GHz and the other six modules observe at 145 GHz. In the simulations of this project only the modules observing at 145 GHz will be simulated, since the 220 GHz module is used for the separation of the foreground, which is not considered.

Each module has 23 pixels and the sensitivity of the sky signal is determined by the observation integration time per pixel, in table 1.2 is shown the principal characteristics of the detectors (Lee et al., 2021). Each pixel has a single-polarized antenna coupled to a hemispherical lenslet; each hemispherical lens has a diameter of 6 mm, which determines the spacing between the detectors. The signal received from the antenna is transmitted to the MKID, and the MKID detects the intensity of the photon in two directions(Choi, 2015; Kutsuma, 2021).

	145 GHz	220 GHz
Number of detectors	138	23
sky coverage	0.537	0.462
Mean observation time (s/arcmin ²)	0.83	0.97
NET ($\mu\text{K}\sqrt{\text{s}}$)	820	2600
pixel noise level ($\mu\text{Karcmin}$)	110	780

Table 1.2.: The table shows calculations for the two principal observation frequencies. The telescope will observe half of the full-sky, for 3 years, with an efficiency of 70%. Also, the NET (Noise Equivalent of Temperature) was calculated following restrictions of the atmosphere and the detectors Lee et al., 2021

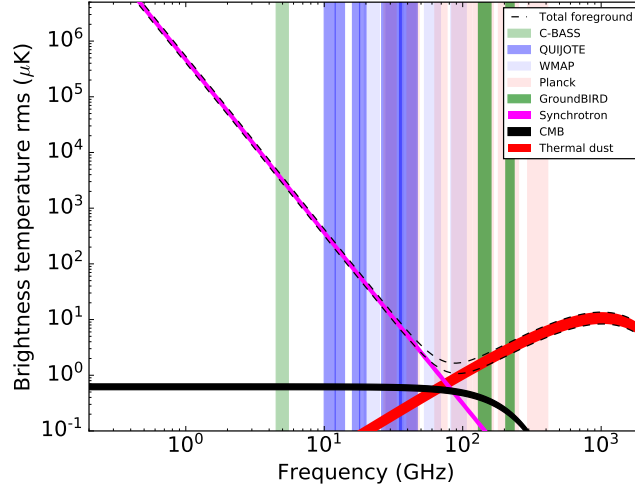


Figure 1.5.: Spectral characteristics of foregrounds and CMB in polarization. Magenta band shows polarized synchrotron emission, and red band polarized the thermal dust emission. The widths of the synchrotron and thermal dust bands are defined by the largest and smallest sky coverages (Jones et al., 2018) updated version with Quijote and GroundBIRD

1.2.2. Simulations: TOAST framework

Radio and microwave sky maps are obtained before the telescope takes real data thanks to software simulations. Software simulation consists of constructing a time-ordered data or TOD object based on the properties of the telescope.

This object represents the measurements of sky signals obtained by the instrument as a function of time, and is also based on certain coordinates, noise parameters and atmospheric conditions. Radio telescope simulations are important for understanding the optimal configuration of the telescope and its instruments (Guidi et al., 2021; Kurki-Suonio et al., 2009), i.e., telescope motion, receiver positioning, recorded data and the resulting sky maps.

The TOAST framework is software that simulates and processes time-streaming data collected by CMB telescopes. Toast simulates detector data with time-correlated noise, and correlated signal sources from the instrument and environmental factors. To estimate the sky signal it is necessary to take large amounts of data and analyze them simultaneously.⁶ That is why TOAST uses internal C++ libraries for optimizing computations and the public interface is written in Python. TOAST uses tools to distribute the data among many processes, performing operations on local parts of the data, filtering, mapping and basic classes to perform I/O see figure 2.2.

This software has been created by Theodore Kisner, Reijo Keskitalo, Andrea Zonca,

⁶https://toast-cmb-kisner.readthedocs.io/_/downloads/en/stable/pdf/

Giuseppe Puglisi, Nestor Demeure and Kolen Cheung in response to the need to better interact with scientific instruments. This has been made possible by improved support for Python on HPC (High Performance Computing) systems⁷⁸.

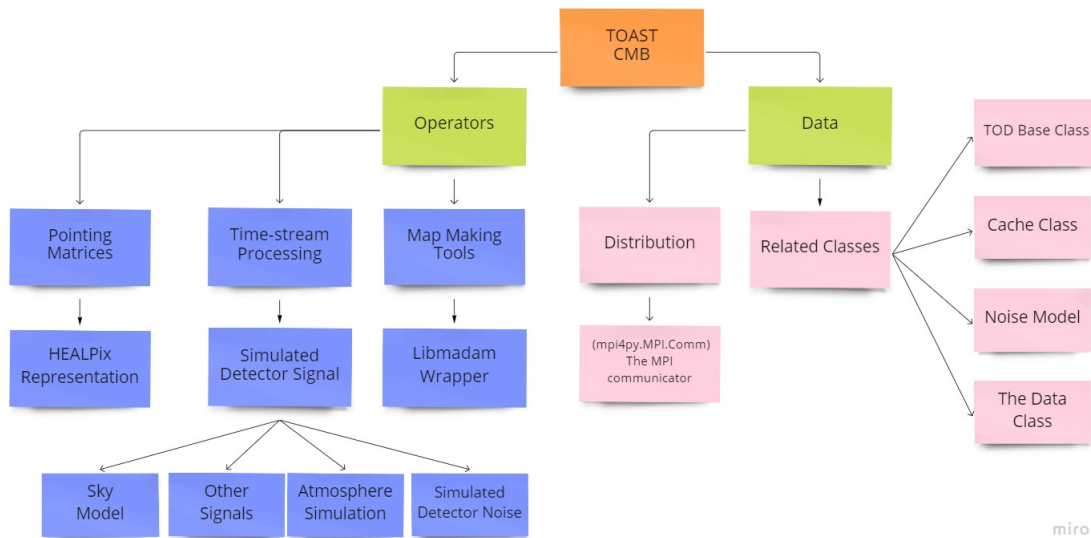


Figure 1.6.: Flowchart of the principal classes of the TOAST framework. Figure shows that TOAST is divided into "Data" and "Operators". Data is related to how TOAST manages different data (TOD object, cache, noise), and Operators are functionalities that use Data and generate some results.

The framework works with data organized into observations. Each observation is independent of any other observation, and each observation contains detectors co-sampled over some time span. TOAST is described by a set of classes, and its processing is distributed among MPI processes. Each observation in the code base is a dictionary that has at least one member named "TOD".

This TOD object is created by entries such as:

- The detector names for the observation.
- The number of samples in the observation.
- The geometric offset of the detectors from the boresight.
- Information about how detectors and samples should be distributed among processes (*mpi4py.MPI.Comm*)

The "end-to-end" simulations of radio telescope observations: from telescope movements/scanning strategy to sky mapping, have a major impact on telescope design and configuration.

⁷<https://toast-cmb.readthedocs.io/en/latest/data.html>

⁸<https://toast-cmb.readthedocs.io/en/latest/operators.html>

This is particularly relevant for cosmological observations, which require very-high sensitivity maps over large parts of the sky. (Guidi et al., 2021)(Kurki-Suonio et al., 2009). In this project, the main code uses TOAST classes shown in the table A.2 in appendix A.

1.3. Objectives

As mentioned, creating simulations of radio telescopes is an advantage, since it allows us to change parameters and observe how the CMB output maps change. In this project, we will simulate the GroundBIRD (Ground-Based Background Imaging Radiation Detector) telescope by creating a virtual radio telescope with Python code.

This will be carried out using the toast-cmb framework, developed by Theodore Kisner and Reijo Keskitalo in Python and C++ software. This code was created to support CMB missions such as Planck, LiteBIRD, Simons Array, Simons Observatory, CMB-S4^{9,10}. We will create a functional software code that simulates the main features of the GroundBIRD telescope and change telescope parameters in the simulation to generate sky maps, time streams, and the Power Spectrum of the resulting maps.

With these results, it will be observed and analyzed how the maps and their power spectrum change; especially for the resulting polarization maps, since the GroundBIRD telescope aims to measure very low power polarization signals. The resulting simulations will be compared to a theoretical input CMB signal obtained from the Planck Public Data Release 3 Mission Ancillary Data files.

In chapter 2, the methodology created to generate the software simulations, the relevant concepts, and basic diagrams to create a functional software code will be described. The chapter 3 will show the results obtained explaining the three code files created to simulate the radio telescope, and the results generated from this code such as CMB output maps and the Power Spectrum of these maps. Finally, in the chapter 4 we will present the conclusions and future work.

⁹<https://cs.lbl.gov/news-media/news/2017/a-toast-for-next-gen-cmb-experiments/>

¹⁰<https://toast-cmb.readthedocs.io/en/latest/intro.html>

2. Methodology

In this chapter, the methodology used to create the simulation code will be described. It will briefly show how the code have been created, how simulations have been running and what are the computational resources used for this. Subsequently, the TOAST classes and parameters necessary to obtain the final results will be presented, as shown in figure 2.2.

2.1. Simulation computational resources

First of all, to create the simulation, the main repository of the TOAST framework ¹ was explored, in which tutorials on the `ipynb` extension file were found. Based on these tutorials, a code containing the main features of the GroundBIRD telescope was developed. This Github repository <https://github.com/angelaarriero/ULLmasterTOASTcode.git> contains the code developed to generate the simulations. Three files `main` code, `TOD` code and `Classes` code needed to run the simulations were used. The resulting code will be discuss in chapter 3.

The TOAST framework offers a public interface in Python. In this way, an environment for Python3 was created on the IAC computers in which the TOAST-CMB package was installed. Other major packages such as HEALPix ², `mpi4py` ³, and PySM3 ⁴ were also needed. The results in this project were obtained using the `healpy` and HEALPix package (Górski et al., 2005; Zonca et al., 2019)

The simulation ran for 24 hours of observation since this is the minimum time to cover the entire sky area necessary to generate the simulations. This processing takes about 5 hours to simulate an input CMB map + Noise (thermal or $1/f$). It means that three years of observation could take around 228 days of simulation or 7.5 months. Figure 2.1 shows some screenshots taken in a running simulation.

2.2. Code development

Figure 2.2 shows four modules in which the general structure of the code will be found. Module A shows that it is first necessary to build the TOD object that contains the information about the focal plane of the telescope, the weather information of the place where

¹<https://github.com/hpc4cmb/toast/tree/64c5b434d9fdd74d513419a6279cae5505b35d28>

²<http://healpix.sourceforge.net>

³<https://mpi4py.readthedocs.io/en/stable/mpi4py.html>

⁴<https://pysm3.readthedocs.io/en/latest/>

2. Methodology

```

KiB Mem : 39616224+total, 19127356+free, 16312088+used, 41767788 buff/cache
KiB Swap: 2097148 total, 2097148 free, 0 used. 23034931+avail Mem

  PID USER      PR  NI   VIRT   RES   SHR  S  %CPU  %MEM     TIME+ COMMAND
 3071 angela+  20   0 0,150t 0,140t 59808 R 134,3 38,0 92:55.56 python3
 27682 nablenh  20   0 0,10 172g 604784 14730 R 100,0 0,2 143:00.02 python3

```

(a) screenshot 1

```

OpenSSH SSH client
top - 20:57:11 up 9 days, 13:42, 14 users,  load average: 3,09, 2,49, 2,44
Tasks: 866 total,  3 running, 543 sleeping,  0 stopped,  0 zombie
%Cpu(s):  5,2 us,  2,3 sy,  0,0 ni, 92,2 id,  0,2 wa,  0,0 hi,  0,1 si,  0,0 st
KiB Mem : 39616224+total, 46615560 free, 17600790+used, 17353878+buff/cache
KiB Swap: 2097148 total, 2093552 free,  3596 used. 21737772+avail Mem

  PID USER      PR  NI   VIRT   RES   SHR  S  %CPU  %MEM     TIME+ COMMAND
  9118 angela+  20   0 0,168t 0,158t 59956 R 119,8 42,8 263:35.59 python3
 26950 mason+  20   0 6478144 1,075t 38876 R 100,0 0,5 13:46.64 sshd@b...

```

(b) screenshot 2

Figure 2.1.: The figure shows a screenshot of the "TOP" command while a script is running. It is possible to observe data like CPU (Percentage of CPU used by the process), RES (RAM memory used by the process), MEM (The percentage of RAM used by the process, that is, the RES value expressed as a percentage), TIME (total time spent in minutes)

the telescope is located, the noise signal that affects the observations, and restrictions on the simulation. Furthermore, it is necessary to create a pointer matrix that contains information about the output maps (NSIDE size or map resolution, the numbering schemes for the pixels NEST or RING, and the number of maps to output), and the scan strategy of the telescope. This pointing matrix use the TOAST function `OpPointingHpix`.

Module B uses the data provided by the TOD object and the pointing matrix, creating a pixel distribution map with the TOAST function `DistPixels`. This pixel map is also creating aided by a CMB map (needed as input in the simulation) and, finally a hits map is generated as a result. In module C, the sky signal is generated using the distributed pixel map aided by the function `OpSimScan`. A scan of the pixel distribution map is made and with this the time-stream of the sky signal is generated. Once this signal was created, it was possible to simulate the time dependency with the noise using the TOAST function `OpSimNoise()`. Thus, the sky signal is affected by the noise.

Finally, in module D, the process known as Map-Maker provided by the TOAST function `OpMapMaker` is found. The Map-Maker function uses the data provided by the *sky+noise* signal to create a binned map. The Map-Maker then uses this information to remove the low-frequency correlated noise generated by $1/f$ noise, through a process called `Destriped`. TOAST uses an external library called *libmadam* to execute this process in the binned output maps. Thus, the results obtained in this process are destriped maps for intensity and Q-U polarization maps.

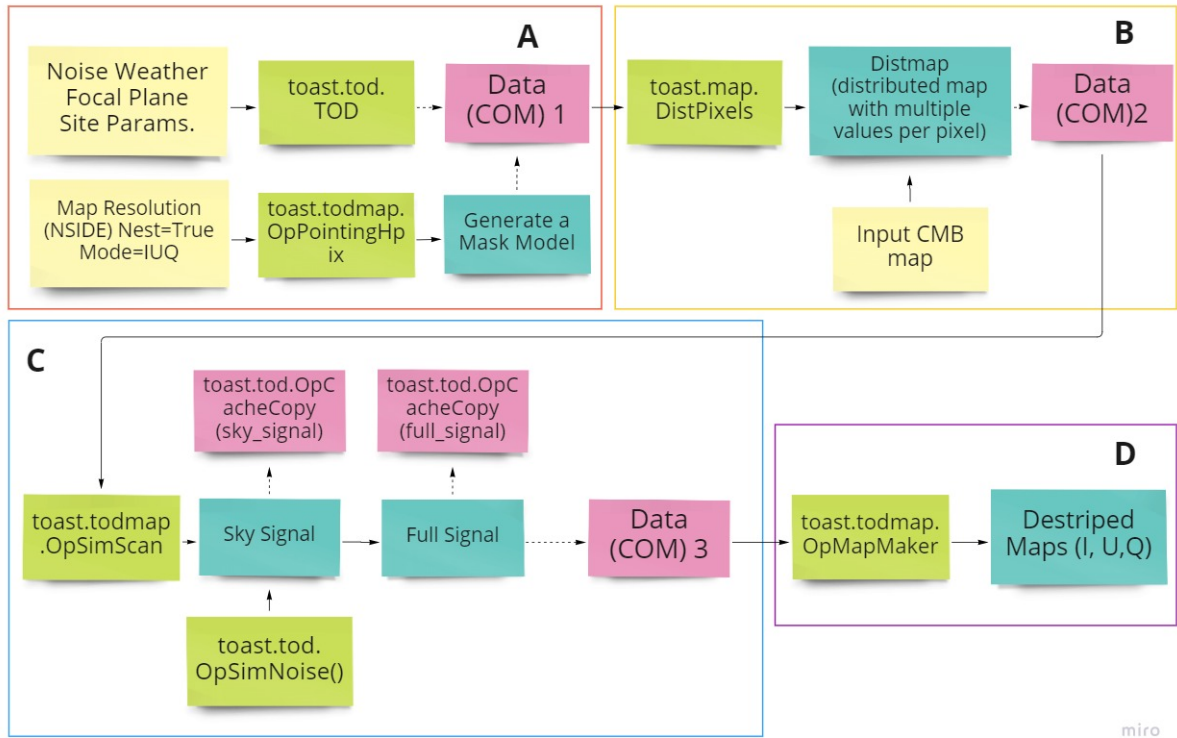


Figure 2.2.: Flowchart showing the modules required to run the code for the GroundBIRD telescope simulation. Module A: the TOD object creation, module B: pixel mask, module C: creation of sky signal according to TOD object and pixel mask, module D: Map-making process.

2.2.1. Module A: Time Ordered Distribution object

The first step is to create a TOD object in the TOAST framework composed of the following elements:

- **Schedule parameters:** These parameters describe the simulation time values, the characteristics of the observing site, and the observing parameters of the telescope.
- **Focal plane:** It is described by parameters such as position, polarization angles, FWHM or beam size, frequency sample rate, and the NET value of each detector.
- **Weather file:** This file contains the meteorological conditions of the place where we want to make the observations to simulate the atmosphere. This file contains the historical distributions of temperature, wind, pressure, and water vapor in a fixed location. This file is sorted by month and hours to capture seasonal and diurnal variations.
- **Noise:** To generate the noisy signal which affects the maps, it was used the Toast function Analytic Noise. This function receives Knee frequency, Net values, detector sample rate, minimum frequency, and the detectors names. With these information, the

function generates a noise signal that depends on time, and simulates $1/f$ noise and thermal noise.

Schedule file, Weather File and Focal plane

GroundBIRD's scan strategy has a constant elevation, periodic motions along the azimuth direction, and a rotation speed of 120 deg/s. With these information and data shown in table 2.1a which presents the parameters used in the simulation, such as the location of the observatory, and the observation window (Duration), it is possible to build the schedule file necessary to create the TOD object.

Variable	Value
Start Time	1577839800.0 GMT: 01-01-2020 0:50:00
Duration	60*60*24 s
Sample Rate	1000 Hz
Altitude	2390 m
Longitude	16°15'16.6" W
Latitude	28°28'05.7" N
Elevation	60 deg
Scan rate	120 deg/s

(a) Scheduler variables

Variable	Value
Quaternions	Pos. and Pol.
FWHM	36' (0.6°)
Spectral Index ($1/f^\alpha$)	1
Sample rate	1000 Hz
Minimum Freq.	0
Scan rate	120 deg/s

(b) Focal plane principal characteristics for simulation

Table 2.1.: Input parameters of the GroundBIRD simulation.

Figure 2.3 shows the hits maps for GroundBIRD Telescope scanning strategy at different hours. The hist maps for the 24 hours show a circle with high n_{hits} . This corresponds to the extra time of 4 minutes that separates a solar date from a sidereal day. To overcome this, we would have to simulate 23h 56min, i.e., a sidereal day, which is the time at which full sky coverage is achieved.

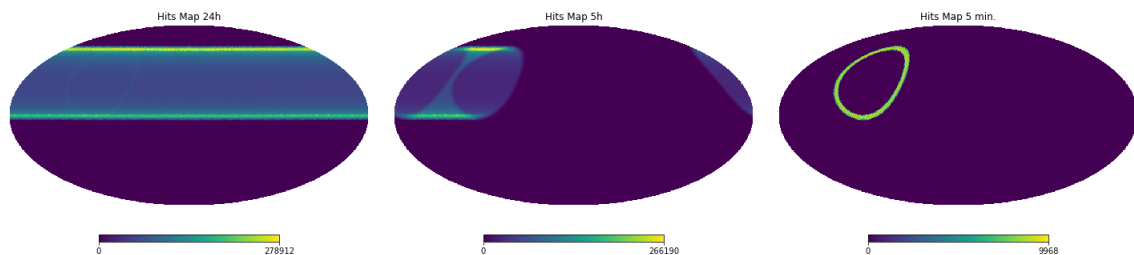


Figure 2.3.: Scan strategy hits maps for GroundBIRD telescope. Figure shows scan strategy when simulation has 24 hours, 5 hours, and 10 minutes of observation time.

2. Methodology

In the other hand, a Fits file generated for Atacama, Chile weather conditions was used in this simulation as principal weather file. This file is available on the NERSC web page⁵. The file was made with data taken from MERRA-2 (second Modern-Era Retrospective Analysis for Research and Applications), a NASA atmospheric database that contains data since 1980. This database includes observations of aerosols from space and represents their interactions.

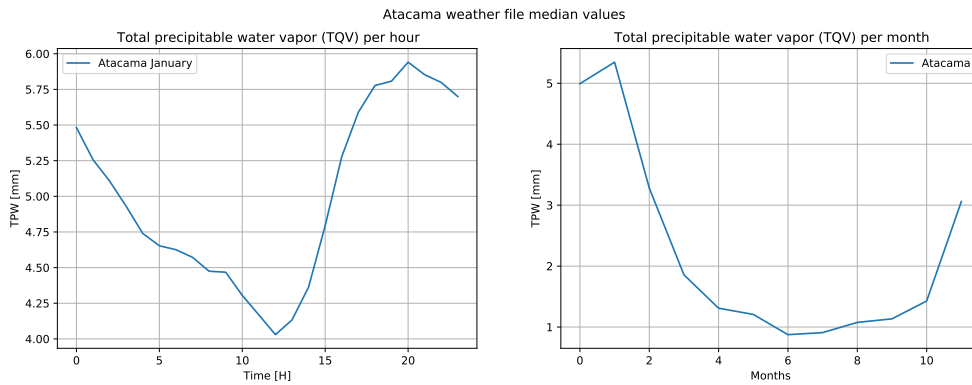


Figure 2.4.: Total precipitable water vapor [mm] for Atacama file. Figure at the left shows the mean values of 12 months for 24 hours and, figure at the right shows the mean value of 24 hours for 12 months of PWV.

The file contains distribution of different parameters for every UTC hour of the day, averaged over months. The parameters taking into account are: TQI (ice water), TQL (liquid water), TQV (total water vapor), QV10M (specific humidity), PS (surface pressure), TS (surface temperature), T10M (air temperature at 10m), U10M (eastward wind at 10m), and V10M (northward wind at 10m)⁶.

The precipitable water vapour is relevant since the water vapour in the atmosphere affects the IR ground observations widely, this because it reduce the signal transmission (atmospheric extinction) in the IR atmospheric window and it produce absorption bands unwanted in the final images. Thus, places where the water vapour content is smaller are the best places to get IR observations. The total amount of water vapour over a place is called PWV or Precipitable Water Vapour which is defined as: "the total height of the water column if integrated from the surface to the top of the atmosphere with unit cross-section"⁷ (Castro-Almazán et al., 2016; Lorenzo et al., 2009; Bustos et al., 2014). Figure 2.4 shows the PWV median values contained in the Fits file of Atacama. January month was selected to run the simulations in this project.

Finally, the focal plane of the telescope consists of 7 hexagonal modules and each module contains 23 detectors or pixels with a fixed position. Figure 2.5 shows the distribution of

⁵https://portal.nersc.gov/project/cmb/toast_data/example_data/

⁶<https://github.com/hpc4cmb/toast/blob/64c5b434d9fd74d513419a6279cae5505b35d28/src/toast/weather.py>

⁷https://glossary.ametsoc.org/wiki/Precipitable_water

those pixels in the focal plane.

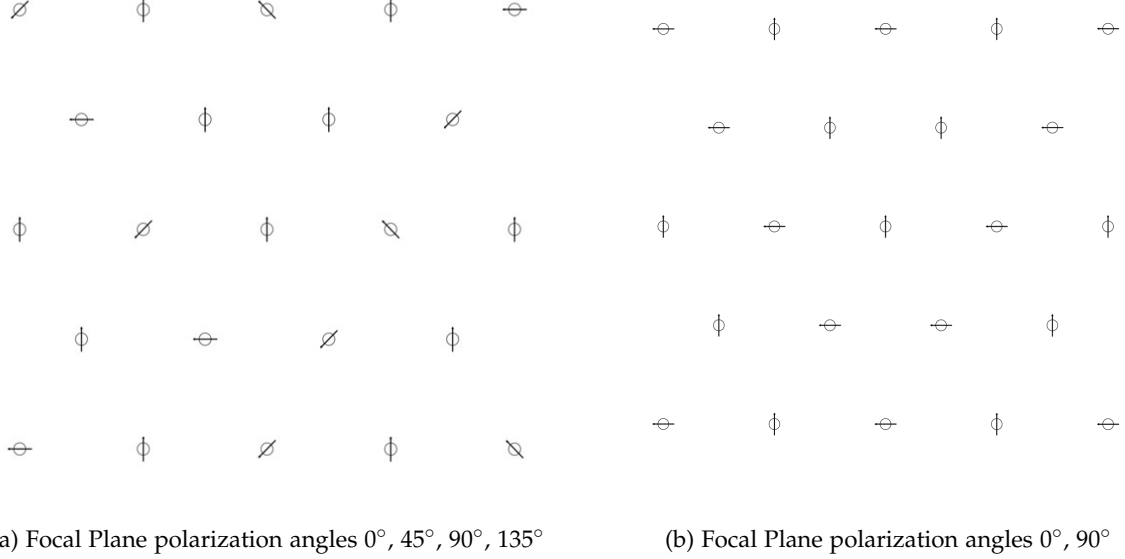


Figure 2.5.: Figure shows the spatial distribution or geometry of the 23 detectors in a module. Furthermore, the polarization angles of each detector are indicated with an arrow.

Noise

The maps will be affected by three noisy signals, which will be injected as input noise to create the maps. The $1/f$ noise, the thermal noise, and a "zero noise" approximation. The thermal noise is a frequency-independent term generating by random fluctuations and appears at high-frequencies. On the other hand, the noise related to the low frequency is called $1/f$ noise, which is generated due to instrumental effect, and because of atmospheric emission.

This signal is usually correlated between detectors, whereof generates significant low frequency excess (Poletti et al., 2017), so it is a frequency dependent-term. This term is a Power Spectrum Density (PSD) noise type with the form $S(f) \propto 1/f^\alpha$ where α identifies the $1/f$ noise type. If $\alpha = 1$ the noise is a pink/flicker noise, which is in most cases (Liccardo et al., 2021)(Lee et al., 2020). Finally, it is important to mention that the "zero" noise is a signal with a low NET value and not is completely zero, since the "zero" value is not executed in the TOAST framework, so to simulate the TOD object in a "zero noise" condition we are using a low NET value.

To execute the simulations, it was created a function to change the knee frequency and the NET (Noise Equivalent Temperature) values to obtain the desired noise. In general we assume that the total noise behaves as Gaussian process, and it can be described by a Power

Spectral Density PSD as is shown in equation 2.1 (Sutton et al., 2009; Delabrouille, J., 1998).

$$PS(f) = \frac{\sigma^2}{f_{sam}} \left[1 + \left(\frac{f_{knee}}{f} \right)^\alpha \right] \quad (2.1)$$

where σ^2 is the white noise variance of a single observation, f_{sam} is the sampling frequency of the detectors, f_{knee} is a "knee frequency" or a frequency in which the thermal noise and low-frequency noise contribute statistically equal to the power spectral density. The spectral index α (between 1 and 2.5) depends on the dominant physical process which is generating the low frequency noise (Sutton et al., 2009; Delabrouille, J., 1998).

Employing the equation 2.1 which is in the module of TOAST called "Analytic Noise", we can get the PSD (Power Spectral Density) for the three signals which will affect the maps. TOAST module takes σ^2/f_{sam} value as the NET value of the detector.

In the other hand, the Noise Equivalent Temperature NET measures the sensitivity of a thermal radiation detector in infrared or microwaves. The NET value is the minimum detectable temperature coming from the incident signal that would be needed to match the internal noise of the detector, so the signal-to-noise ratio is equal to one (Sutton et al., 2009). When intensity and temperature relation are well defined in a pass band, it is possible to scale NET with NEP (Noise Equivalent Power), that is the case of a blackbody ^{8,9}.

The GROUNDBird experiment uses NET 820 $\mu\text{K}\sqrt{\text{s}}$ for each MKID detector. This value was calculating based on the detector MKID characteristics and the atmospheric characteristics of the place where the detector is placed (Tenerife, Canary Islands). To estimate this value, we can calculate the Noise Equivalent Power given for the equation 2.2, and then scale the NET value (Lee et al., 2020).

$$NEP^2 = \frac{1}{\eta_{opt}} \int d\nu \left[2h\nu P_{rad}(\nu) \{1 + \eta_{opt} \eta_{em}(\nu) \bar{n}_{bb} F(\nu)\} + \frac{4\Delta}{\eta_{pb}} P_{rad}(\nu) \right] \quad (2.2)$$

Moreover, figure 2.6 shows the time-stream and power spectral density (PSD) of the thermal, 1/f and "zero" noise signals to be applied to the simulation. Their main characteristics are listed in table 2.2a. The thermal and "zero" noise will be maintained in all simulations, while the knee frequency of the 1/f noise will change.

⁸https://www.lasercomponents.com/de/?embedded=1file=fileadmin/user_upload/home/Datasheets/lc/application-reports/lc-pyros/calculation-net.pdf&no_cache=1

⁹<https://en-academic.com/dic.nsf/enwiki/11786911>

2. Methodology

Signal Noise	Knee freq.[Hz]	NET[$\mu\text{K}\sqrt{\text{s}}$]
Zero	0	0.001
Thermal	0	820
1/f	10	820

(a) Characteristics of noisy signals. Values such as knee frequency and NET will change in some simulations.

Variable	Value
NSIDE	64
Ordering scheme	Ring
NNZ	3

(b) Values to build the pixel distribution map for the simulation

Table 2.2.: The tables show the principal signals which will affect the simulated maps with their characteristics, also shows some values required to construct the pixel distribution map like NNZ (values per pixel), and Nside (resolution of the grid) (Gorski et al., 2005).

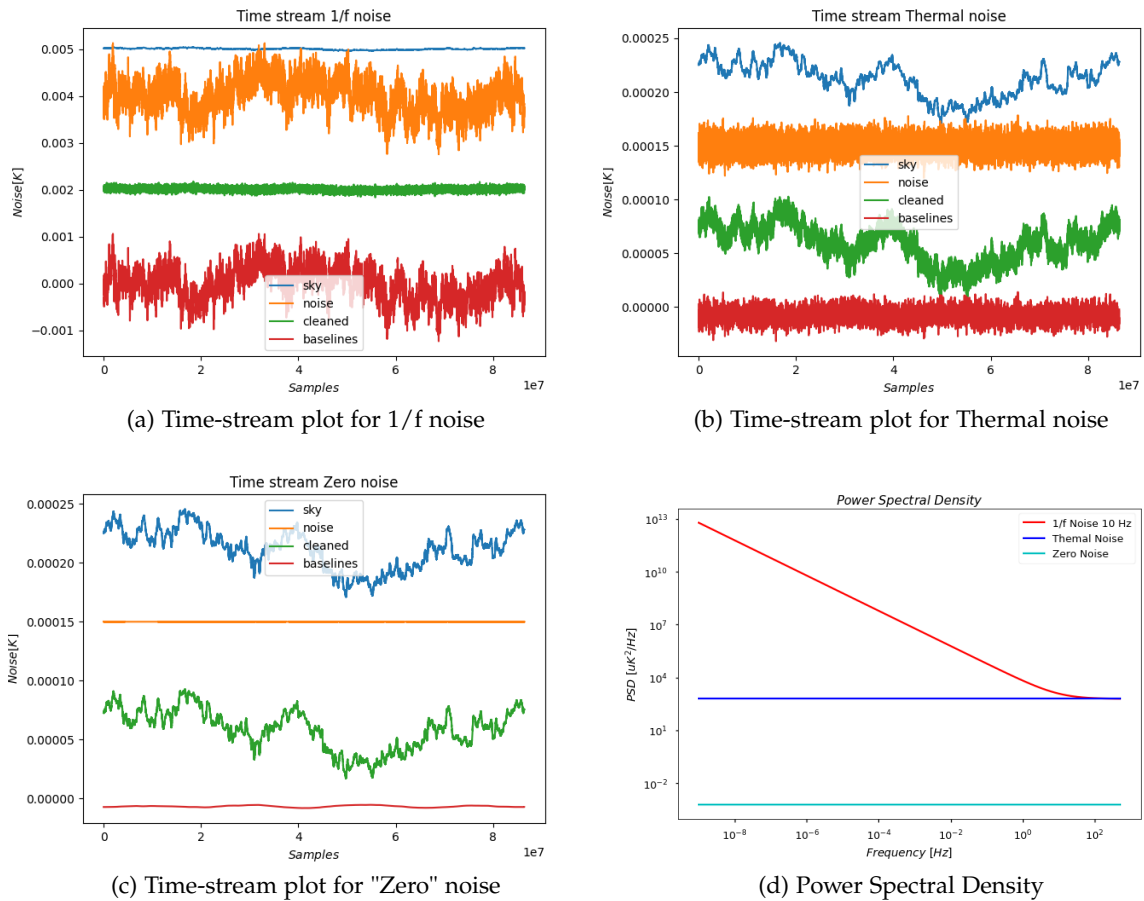


Figure 2.6.: Time-streams and PSD (Power Spectral Density) for 1/f noise at knee frequency 10 Hz, Thermal Noise, and "zero" noise.

Finally, once the TOD object is building, the pointing matrix must be created using the TOAST function called `OpPointingHpix`. This function generates pointing weights for I-Q-U that depend on the individual pointing of the detector. This matrix is created by the TOAST

function using the TOD object information and the resolution parameters specific to Healpix library. Table 2.2b shows the parameters chosen to perform the simulations.

2.2.2. Module B: DistPixel Function

Once the TOD object has been constructed and the pointing matrix has been defined, it is necessary to create a distribution map with multiple values per pixel, i.e. each process has a local data storage in one or several sub-maps. This requires an input map, and in this case we will use a CMB map in FITS format to be used as the input signal.

It was taken a CMB model created by Andrea Zonca in the web page "Read and process Planck CMB power spectra with healpy" ¹⁰.

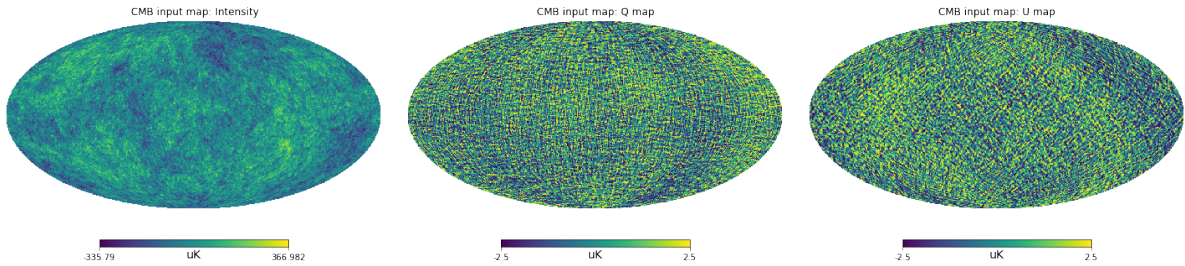


Figure 2.7.: Figure shows the CMB map chosen as input or model to feed the simulation. This CMB map contains the Intensity, and polarization Q-U maps.

This model is shaped by cosmological parameters measurement by Planck ¹¹, and table A.3 shows these principal parameters. The spectrum is found into the Ancillary data section, and figure 2.7 shows the maps generated for simulate I, Q, and U maps. This model allow us to change parameters in the input CMB map, and with this we can choose the Gaussian beam (fwhm) to smooth the map, and the NSIDE to change the angular resolution of the map. Appendix shows the result power spectrum to FWHM (0.1, 0.6, 0.8) and NSIDE (64, 256, 1024).

The GroundBIRD telescope has two observing frequencies: 145 GHz and 220 GHz. The angular resolution for each frequency is 0.6° and 0.4° respectively, calculated with the equation 2.3, where D is the aperture window (220 mm).

$$\theta_{FWHM} = 0.89 \frac{\lambda}{D * 57.29^\circ} \quad (2.3)$$

For this simulation, the detector will be simulated at 145 GHz, so the maps will be smoothed with a Gaussian beam at 0.6° FWHM. (Lee et al., 2020).

¹⁰<https://zonca.dev/2020/09/planck-spectra-healpy.html>

¹¹https://irsa.ipac.caltech.edu/data/Planck/release_3/ancillary-data/cosmoparams/COM_PowerSpect_CMB-base-plikHM-TTTEEE-lowl-lowE-lensing-minimum_R3.01.txt

2.2.3. Module C: Sky signal and Full signal

The TOD object has been created in a pixel distribution map, and the next step is to use the function called `OpSimScan` to generate the sky signal corresponding to this TOD object. Although the TOD object contains the noise property, in this step the sky signal is created and the noise does not yet affect this signal.

After creating the sky signal, the TOAST function will affect the sky signal to simulate a real observation. The function generates noise time streams for each detector and observation based on the noise object of the current observation. Finally, the TOD object is represented by a sky signal, which is affected by a noise signal manipulated by the user.

Figure A.2 shows some examples of time-streams sky and noise signals that the user can obtain. These signals belong to a 10-minute simulation. Orange represents the sky signal, blue is the noise signal (1/f or thermal noise), and green represents the baseline signal, i.e. the signal obtained after the map destriping process. The sky+noise signal generates a "full signal", which is the input signal to the TOAST mapping function.

2.2.4. Module D:Map-making

Once the full signal (sky+noise) is created, the TOAST framework offers a function called `OpMapMaker` whose input parameter is this "full" signal. This function creates the binned map, and with the help of the `Libmadam` library these binned maps are processed to remove the correlated signals present in the maps, and thus generate the destriped maps to analyze the final results. The TOD object consists of a sky signal and a noise term:

$$d = Pm + n' \quad (2.4)$$

where the first term represents the CMB signal and the second one is the noise. m is a vector which represents the pixelized CMB+foreground map, P is a pointing matrix which distributes these map into the TOD. P is a matrix with columns I,Q, and U for each sky pixel. Map m includes polarization, so m is an object of $3N_{pix}$ elements and N_{pix} is the number of sky pixels. That means, the map contains three values per pixel which represents the Stokes paramters I,Q,U (Poletti et al., 2017; Keihänen et al., 2010).

Map-making process is used to calibrate the time-ordered data recorded by the detectors, and this time samples are collected in a vector d . To model how the sky signal contributes to each time sample collected, we need to know about the scan strategy of the telescope and the polarization modulation. The observed signal is shown in equation 2.5(Poletti et al., 2017; Keihänen et al., 2010).

$$d_t = I_P + \cos(2\phi_t)Q_P + \sin(2\phi_t)U_P + n_t \quad (2.5)$$

where n is the noise, I, Q , and U are the Stokes parameters of the incoming light for the sky pixel P observed at time t , and ϕ is the orientation of polarization sensitivity which depends on the detector's position in the focal plane. The factors $1, \cos(2\phi_t), \sin(2\phi_t)$ forms the pointing matrix P .

The noise contribution is divided into a correlated noise part and white noise, where the correlated part is model as a sequence of uniform baselines, so $n' = Fa + n$, where a is a vector which contains random amplitudes of the baselines, and F is a matrix which indicate which samples belong to which baseline into the TOD object (Poletti et al., 2017; Keihänen et al., 2010).

The $1/f$ noise component (correlated noise) needs to be removed from the signal doing a destriping process. If the signal is not removed some ring patterns will remain. This patterns come from instrumental variations, change in atmospheric conditions, and the scan strategy (Lee et al., 2020). TOAST has an interface with a destriping library called *Libmadam*, this library approximates that the covariance between the F matrix is stationary and can be calculated from the detector noise power spectral densities (Poletti et al., 2017; Keihänen et al., 2010)¹². This is a library version of the *MADAM* map-making code. Finally, the TOAST framework generates a series of resulting maps, which can be further analyzed.

- Hits map
- Binned Map
- Destriped Map

¹²<https://portal.nersc.gov/project/cmb/toast-tutorial/05MapMaking/mapmaking.html>

3. Results and Discussion

In this chapter, the results of the project will be discussed. The first result is a python code that uses the TOAST framework to simulate the GroundBIRD radio telescope; then using this code we will change telescope parameters such as *Integration time*, *Focal plane*, *Detector NET value*, *Knee frequency* of the 1/f signal affecting the telescope, *Elevation*, and *Scan strategy* to analyze the CMB maps and its power spectrum result.

3.1. Virtual Radio Telescope

The virtual radio telescope generated for the GroundBIRD telescope is programmed in Python3 using the TOAST framework. We have created 3 files and this code is located in the following Github repository <https://github.com/angelaarriero/ULLmasterTOASTcode.git>.

The file **Main code**¹ contains the main function and from here we call two more files where the properties of the telescope and the characteristics of the site are specified (**from TODangela import (TODGb)** , and **import classesDef as cd**). Next, we need the input map that will be used as a model to generate the simulations. In this project, we use a *.txt* file containing a power spectrum taken from the PLANCK website and using

```
def cmbinput(Dsimulation)
```

function, we obtain a *.fits* file which represents the map generated by the power spectrum. The values *NSIDE* and *FWHM* are needed to build the map.

Next, some corrections are made to the original file containing the position of the detectors in the focal plane by changing the polarization angles. This file was provided by the GroundBIRD group. Now, once we have the requirements set, we generate the noise function that will affect the maps. To do this, we use the function

```
N2=cd.minoise(cd.Ddetector,250,1)
```

The first parameter is the detector characteristics class, then the knee frequency, and then the NET value. These values are scale factors, so in this case, these values represent a signal with knee frequency at 1Hz and NET value specified in the *class Ddetector:detnet* value.

The principal function is

¹<https://github.com/angelaarriero/ULLmasterTOASTcode/blob/main/Main%20code>

```
Noise2,data2=cd.mifuncion(cd.Ddetector,cd.Dschedule,N2,weth_fil,cd.focalplane,MAPA_SIM,cd.Dsimulation,outdir2,outprefix2)
```

This is composed of the detector and schedule characteristics, the noise which we want to apply, a weather *.fits* file, the focal plane geometry and working characteristics, the input map, and the characteristics of the simulation to generate the output maps. We expect the values Noise2 and data2, and with those values, we can plot time-streams graphics of the noise and other signals which affects the maps. Also, TOAST generates *.fits* files with the binned and destripping maps resulting from the TOD object.

The file **classesDef** ² contains functions and classes. The classes are: *class Dschedule* (simulation time and site values), *class Ddetector* (principal characteristics of the detector), *class Dsimulation* (values to generate the output maps); and functions as:

```
def Dknee(Ddetector,number,n2)
```

This function set the desired knee frequency and NET values, and then with the next function create a function noise expected by the user.

```
def minoise(Ddetector,numberD,n2)
```

This function use the TOAST analytic noise function to generate noise

```
def mifuncion(Ddetector,Dschedule,noise_ar,weather_atacama,focalplane,MAPA_SIM,Dsimulation,outdirD,outprefixD)
```

This function create the TOD object, the sky signal, simulate the noise affecting the sky signal, and at the end the Map-Maker process is done to the signal affected by the sky and the noise,

```
def cmbinput(Dsimulation)
```

This function generate the input CMB map, here is needed to use a Power Spectrum file to then obtain the CMB model in a fits file.

To generate the TOD object, the function *TODGb* is called. This function is found in the **TODangela** ³ file. This file is modified from the original found in the TOAST library. Here, we specify the scan strategy of the telescope with the function

```
def simulate_scan(self, samples,e1)
```

Here, we define that elevation is constant and the maximum and minimum azimuth movements. In general, this file constructs the schedule or specific time at which the telescope will point based on the simulation time, the simulation month and the scan strategy.

The next sections show the results generated using the above code. These results simulate general telescope conditions, and basic parameters are changed to observe the results.

²<https://github.com/angelaarriero/ULLmasterTOASTcode/blob/main/classesDef>

³<https://github.com/angelaarriero/ULLmasterTOASTcode/blob/main/TODangela>

3.2. Integration Time

Initially, the simulation run for 24 hours of observation. Nevertheless, due to the detector conditions, to get an optimal noise level, the telescope will observe for three years. Higher computational resources and execution time are require to run three years of observation.

To handle this, as the simulation runs for 24 hours, the sensitivity per \sqrt{s} is rescaled to one year based on the number of days. In this case, the detector noise $NET\ 820\mu K\sqrt{t}$ is rescaled by assuming that this is the NET value of a detector for 24 hours of observation. This NET value belongs to the detectors observing at 145 GHz shown in the table 1.2). Thus, the noise level is scale down as is shown in the equation 3.1 for three years of observation and one detector.

$$\frac{820\mu K\sqrt{s}}{\sqrt{3 * 365 * 1}} = 24.78\mu K\sqrt{s} \quad (3.1)$$

The thermal noise can be reduced as the square root of the integration time, but $1/f$ noise cannot be reduced as thermal noise. To check how the $1/f$ noise is reduced, it is necessary to perform longer runs, e.g., a week or a month of data and plot the RMS value as a function of integration time to observe if it is reduced as \sqrt{t} , however, this requires a lot of computational time. Therefore, in these simulations, we will assume an optimistic scenario of the value of the $1/f$ noise for three years, mainly because we want to show the main effects of this $1/f$ noise over the telescope simulations compared to the thermal noise.

In this test, we will see the CMB maps output when the NET value is $820\mu K\sqrt{s}$ and $24.7\mu K\sqrt{s}$, or 24 hours and 3 years of integration time for a single detector. As we mentioned in section 2.2.1, we will simulate three types of signals which will affect the maps: thermal noise, $1/f$ noise, and a very low thermal noise called "zero noise". Figure 3.1, shows the output maps when we change the NET value of one detector. We find in the figure two kinds of maps: **Binned map** and **Destriped Map**. The "Binned map" uses a "Hits map" (see figure 2.3) to build an intensity map according to weather conditions, noise (e.g., $1/f$ noise, thermal noise), focal plane, and the geography site characteristics. In the end, we have a map that contains all these observational restrictions.

On the other hand, the destriping map is the result of removing or "Destripe" the correlated low-frequency noise present in the Binned map, generated due to the $1/f$ noise (these correlations can be seen in the Binned map). This "Destriping" process will not remove the thermal noise contained in the Binned map since thermal noise is a frequency-independent term as we mentioned before. Furthermore, figure 3.2 shows results for subtractions for 24 hours (a) and 3 years (b) integration time, to get the residual noise of the maps when the resulting destriped map is subtracted from the input CMB map.

Discussion

In figure 3.1, the "zero noise maps" in both cases (24 hours and 3 years) are similar to the intensity map of the input CMB shown in figure 2.7. Since the zero noise is a very low noise value and it is simulating "noiseless", it has the sense that the destriping process will not change the Binned map.

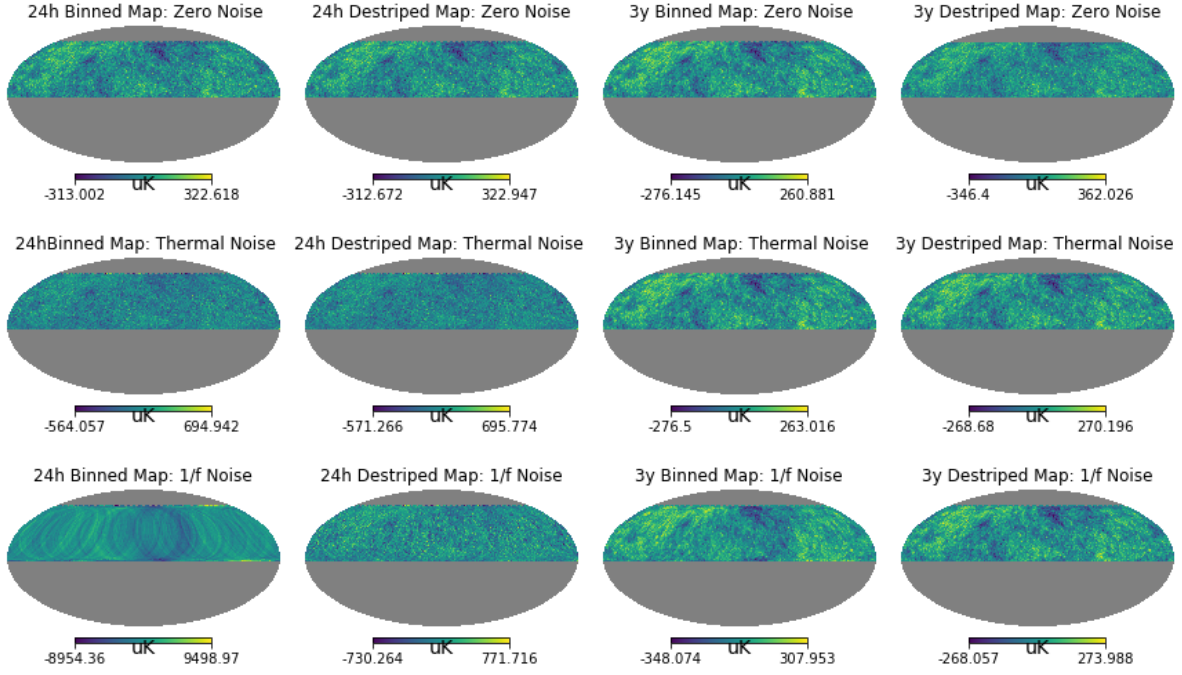


Figure 3.1.: The figure shows the intensity Binned and Destriped maps for observation time of 24 hours (center to the left) and 3 years (center to the right), with NET $820\mu K\sqrt{s}$ and $24.7\mu K\sqrt{s}$ respectively. From top to the bottom, we find the simulation output maps of the "zero", thermal, and $1/f$ noise signals.

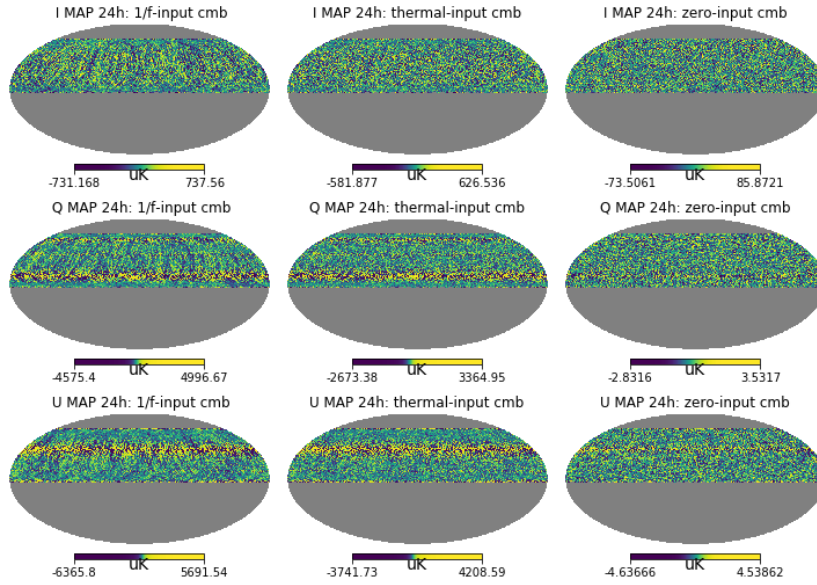
The 24 hours binned map shows that the thermal map is noisy, in which barely we can distinguish structures shown in the input intensity CMB map (or in the zero noise map). Besides, the $1/f$ noise map shows a ring-like pattern very intense, which is generated due to the scan rotating strategy of the telescope and the $1/f$ noise.

On the other hand, for the three years simulation, thermal and $1/f$ noise Binned maps had been improved compared to the 24 hours simulations. The thermal noise seems to show structures similar to the input intensity CMB map and also to the $1/f$ noise map, nevertheless, structures at 10 Hz knee frequency are still visible.

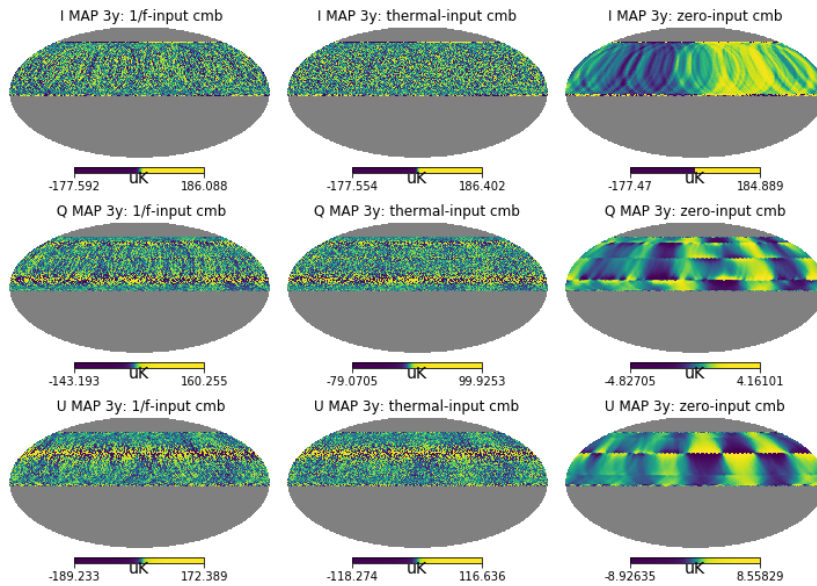
Finally, the Destriped map's output for Thermal and $1/f$ noise in the 24 hours simulation, shows that the "Destriping" process improves the results only for the $1/f$ noise binned map as we thought because this process works for correlated signals; that is why the thermal map is almost the same as we saw in the binned map. Also, the 3 years simulation shows in the

3. Results and Discussion

1/f noise destriped map a cleaner map compared with its binned map, whilst the thermal map remains almost similar to its corresponding binned map.



(a) Simulation for 24 hours of integration time



(b) Simulation for 3 years of integration time

Figure 3.2.: This figure shows the residual maps obtained after subtraction from the destriped maps of the 1/f noise (left), thermal noise (center), and zero noise (right) of the input CMB model signals. At the top, we find the intensity maps, in the center the polarization Q maps, and at the bottom the U maps results.

Furthermore, figure 3.2 (a) and (b), show that the polarization maps have yellow horizontal

lines. This result could appear due to the polarization angles of the detectors in the focal plane (see figure (b) in 2.5) because in the case (a), the focal plane is only cover two polarization angles 0° and 90° . On the other hand, we can also analyze the pixel noise values of the residual maps, and we can see that in 3 years of simulations the pixel noise level is quite lower than the 24 hours maps.

3.3. Focal Plane

The focal plane is crucial in the observations since its geometry, amount of detectors and noise level determine the quality of the results. Figure 2.5, shows the geometry and spatial distribution of the detectors in the focal plane. As the telescope pretends to obtain polarization maps is important to define the polarization angles of the detectors.

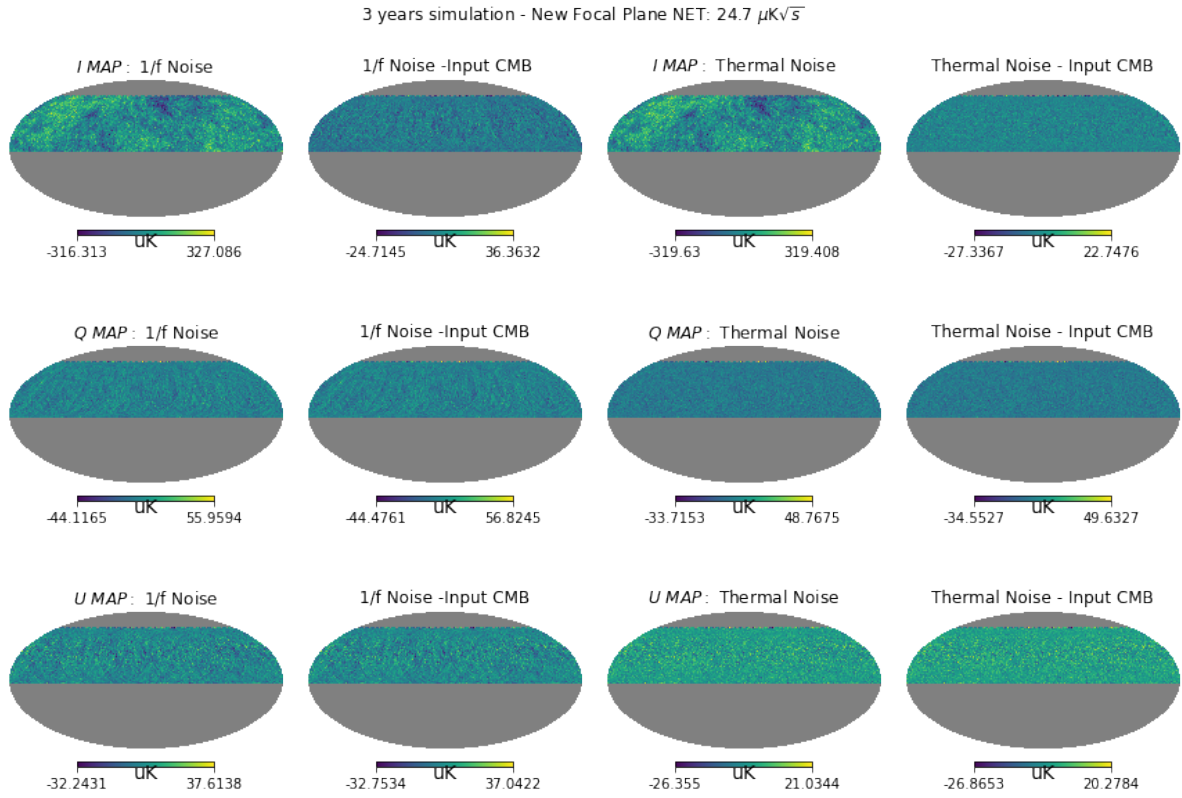


Figure 3.3.: The figure shows the amplitude and residual maps for the 1/f and thermal signals for an observation time of 3 years (NET $24.7 \mu K\sqrt{s}$) with the focal plane which contains polarization angles 0° , 45° , 90° , 135° . At the top, intensity maps, in the center the polarization Q maps, and at the bottom polarization U maps. Column one and three shows the amplitude maps, and column two and four show the subtractions.

Figures 3.2 (a) and (b), show in the polarization maps a yellow horizontal lines very saturated. It is thought that this misbehavior is because the polarization angles used in the

simulation are the ones shown in figure 2.5 (b). So, in this section we will simulate the three years maps (NET $24.7\mu\text{K}\sqrt{s}$) with the focal plane shown in figure 2.5 (a); which contains 4 different polarization angles: 0° , 45° , 90° , 135° .

Furthermore, Figure 3.3 show the output maps generated with the focal plane which presents four different polarization angles (see figure 2.5(a)). We are interested on analyze the Power Spectrum PS (or the Fourier transform) generated from the 3 years' output maps, and figure 3.4 shows the power spectrum plotted. For this project, the Power Spectrum will show three signals generated by the CMB map, i.e., the TT or Temperature PS (Total spectrum), and the polarization anisotropies: EE and BB modes. The output signals will be compared with the input CMB signal used to feed the TOD object of the simulation, and this input signal will be represented by dashed lines.

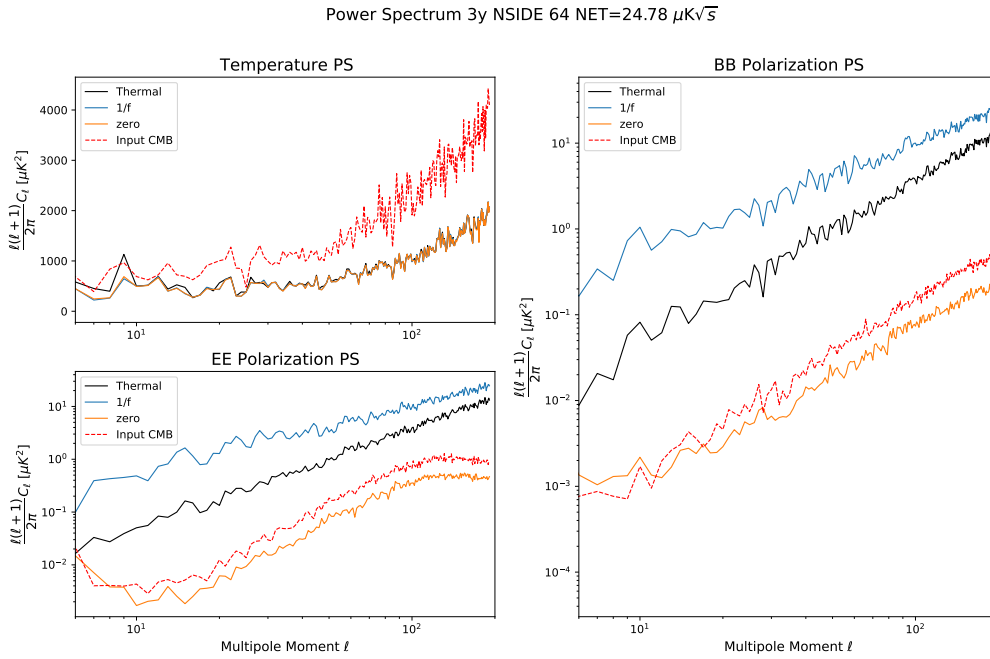


Figure 3.4.: The figure shows the power spectrum PS results of the amplitude maps of figure 3.3 compared with the PS of the input CMB map (in dash-line).

Discussion

Figure 3.3 shows that the horizontal lines now are not present in the polarization maps; and also that the residual pixel noise is quite lower compared with the ones in figure 3.2 (b). Thus, having different directions in the polarization angles allow us to reduce the level of noise for the $1/f$ and thermal noise maps. Also, comparing $1/f$ noise residuals with the thermal noise residual shows that pixel noise is still higher in the $1/f$ maps, and we can see

that Q and U maps are very noisy; so it does not allow us to see the structures present in the input CMB map (see figure 2.7).

Figure 3.4 shows that the temperature TT signal is similar to the input intensity map at very low dipoles. However, the measurements seem to be below the expected signal. On the other hand, the polarization outputs do not follow the form of the expected EE and BB signals of the input CMB model. We can see that thermal and $1/f$ noise draw away in power and form too much, while the "zero noise" signal at least in the polarization signals follows very closer the pattern. From here, all the simulations below will have the new focal plane, i.e., detectors will have four polarization angles.

3.4. NET

As we saw in figure 3.4 the Power Spectrum used for three years of simulation for a single detector (NET value of $24.7 \mu K\sqrt{s}$) does not represent the input CMB signals very accurately. Figure 3.5, shows the results obtained when the NET is $2.5 \mu K\sqrt{s}$. This calculation is shown in equation 3.2, where we have six modules with 23 detectors, observing efficiency 70% in the observations, and three years of observation; the figure 3.4 shows the amplitude and residual maps for this NET.

Furthermore, figure 3.6 shows the Power Spectrum for this NET value, and since the "zero noise" signal is made with a low value of NET "0.001" and Knee frequency "0", to change the NET value in the simulation will affect this "0.001" value, so the results are shown in figure 3.5 (b).

$$\frac{820\mu K\sqrt{s}}{\sqrt{3 * 365 * 23 * 6 * 0.7}} = 2.5\mu K\sqrt{s} \quad (3.2)$$

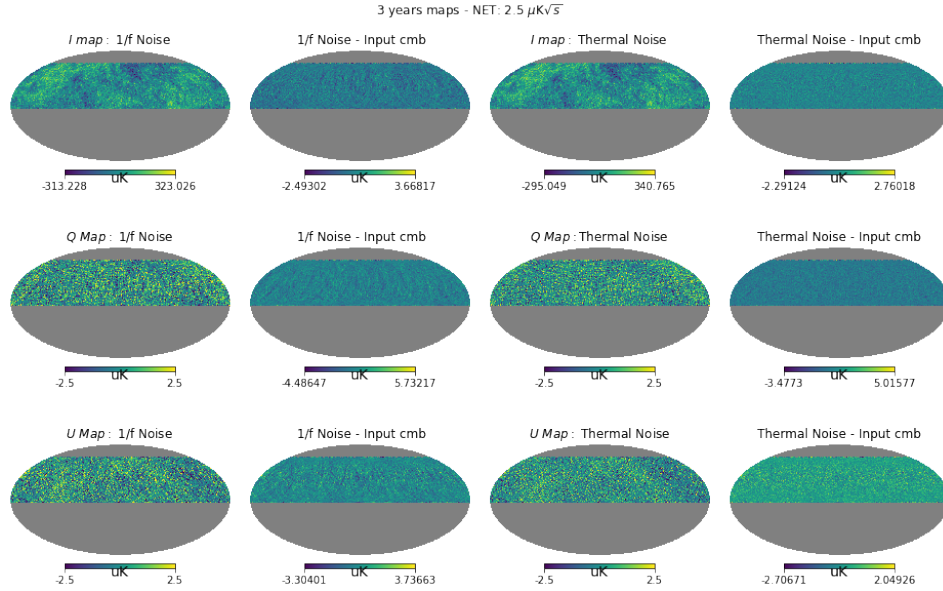
Discussion

Figure 3.5 shows amplitude maps in columns one and three, and compared with figure 3.3 these maps shows that the polarization maps contains some structures, this is because the pixel noise is quite lower at NET $2.5 \mu K\sqrt{s}$. Columns two and four show the residual maps, and how is expected, the pixel noise residual is lower compared with the NET $24.7 \mu K\sqrt{s}$.

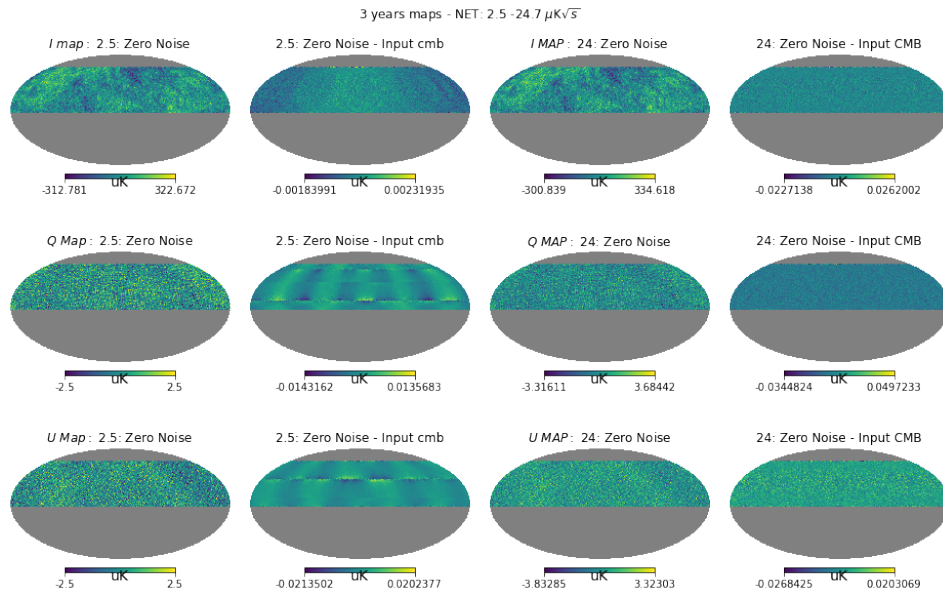
In the other hand, figure 3.6 shows that the output signals have similar form to the input CMB model. Thermal signal has practically the same form as the zero noise signal. However, these simulated signals seem to be below the model. The $1/f$ noise has a knee frequency of 10Hz for the simulation, and despite the signal getting better respect the NET $24.7 \mu K\sqrt{s}$ needs to be improved. Finally, figure 3.5 (b) shows how the noise level decrease when the

3. Results and Discussion

NET value is lower. Structures in polarization maps are more intense and the residuals tend to be zero.



(a) Maps for 1/f and thermal noise NET $2.5 \mu K \sqrt{s}$



(b) Maps for zero noise NET $2.5 \mu K \sqrt{s}$ and $24.7 \mu K \sqrt{s}$

Figure 3.5.: The figure shows the amplitude and residual maps. Figure (a) shows the maps for the 1/f and thermal noise NET $2.5 \mu K \sqrt{s}$, and figure (b) shows the zero noise maps for NET $2.5 \mu K \sqrt{s}$ and $24.7 \mu K \sqrt{s}$. At the top intensity maps, in the center polarization Q maps, and at the bottom polarization U maps. Column one and three shows the amplitude maps, and column two and four show the subtractions.

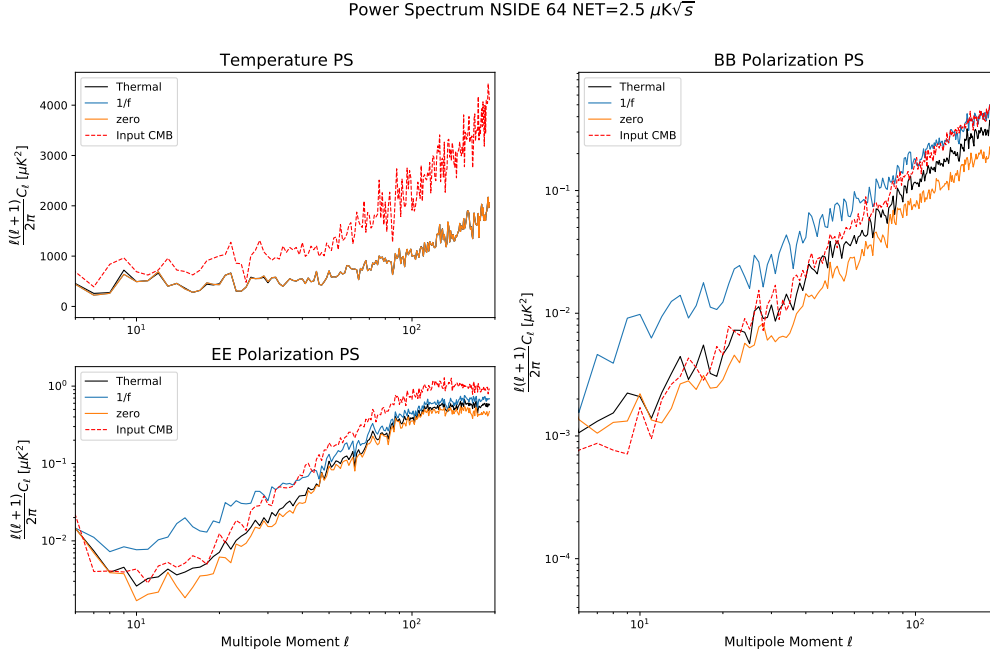


Figure 3.6.: The figure shows the Power Spectrum PS of figure 3.5 maps compared with the PS of the input CMB map (in-dash line).

3.5. Knee Frequency

The $1/f$ noise is a frequency depend noise signal. We will change the *Knee frequency* of the $1/f$ noise signal, and the chosen values are 0.001 Hz, 0.1 Hz, 1 Hz, 10 Hz, 50 Hz, and 100 Hz. The general conditions of the telescope are: elevation of 60° and scan rate 20 rpm. Figure 3.7 (a), shows the results obtained when the Net value is $24.7 \mu\text{K}\sqrt{s}$, and figure 3.7 (b), shows the results when Net value is $2.5 \mu\text{K}\sqrt{s}$.

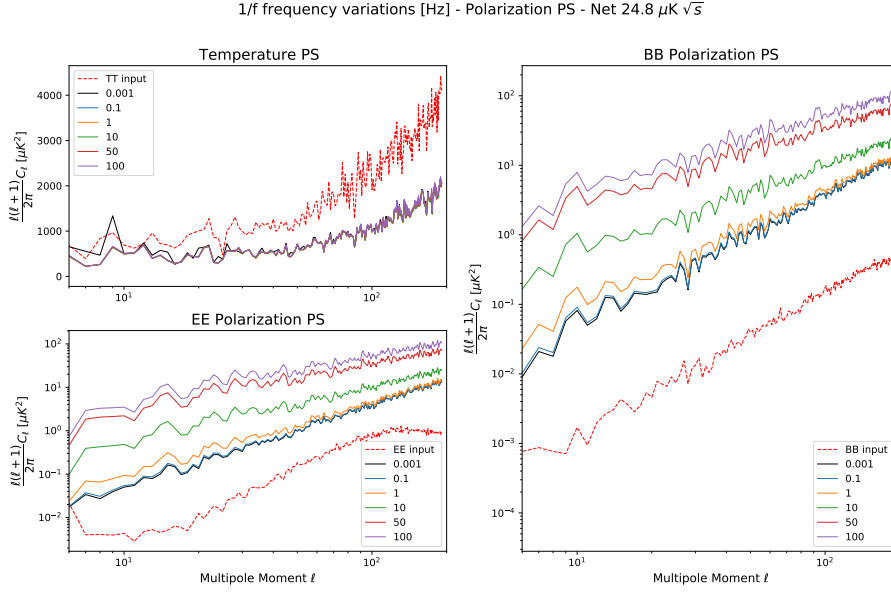
Discussion

Figure 3.7 (a) shows that the knee frequency change the power spectrum amplitude. When the knee frequency is lower the signal seems to be closer to the input CMB signal; however, the effect works for amplitude but does not work in the form. Furthermore, figure 3.7 (b) NET $2.5 \mu\text{K}\sqrt{s}$, shows that in a low knee frequency, the $1/f$ noise signal starts to be less flattened and is similar to the form of the input CMB signal. This is visible for knee frequency at 0.001 Hz and 0.1 Hz.

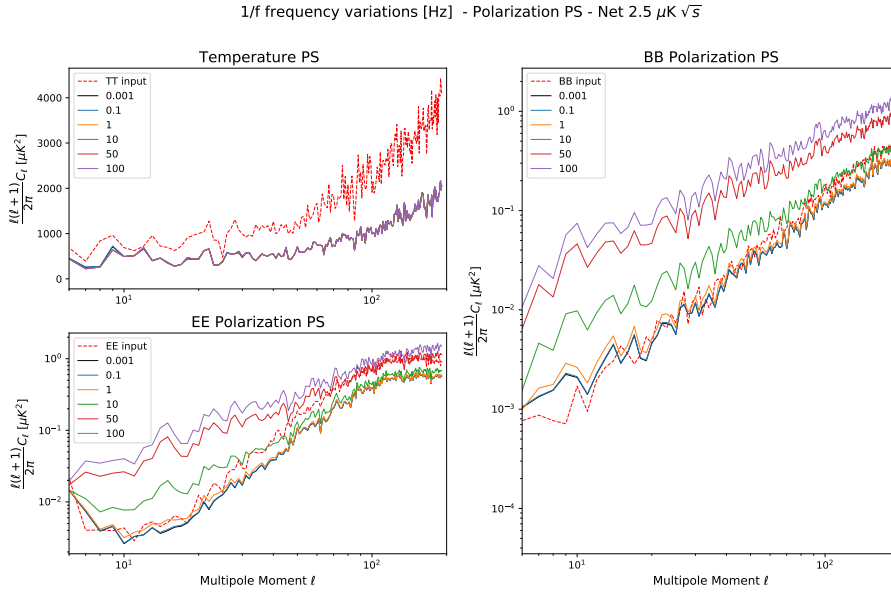
Finally, we can say that the knee frequency hugely affects the power spectrum when this frequency is higher. That is why reduce this value is very important, because at low multi-poles this value become crucial to get the desired signal. From here, the $1/f$ noise signals will

3. Results and Discussion

have default knee frequency of 1 Hz, since we saw it is the frequency which tend to be similar to the desired polarization signals.



(a) Power Spectrum for NET equal to $24.8 \mu\text{K} \sqrt{s}$



(b) Power Spectrum for NET equal to $2.5 \mu\text{K} \sqrt{s}$

Figure 3.7.: The figure shows the power spectrum PS results for TT, EE, and BB modes when the $1/f$ noise has a knee frequency of 0.001 Hz, 0.1 Hz, 1 Hz, 10 Hz, 50 Hz, and 100 Hz compared with the PS of the input CMB map (in-dash line). Telescope elevation of 60° and scan rate 20 rpm

3.6. Elevation

GroundBIRD telescope has a minimum elevation angle of 60 degrees. Since mass of air changes with the observation elevation, the radiation power received from the sky will vary. Figure 3.9 (a) and (b) shows the power spectrum when five elevation angles are simulated: 40°, 50°, 60°, 70°, and 80° for the three noisy signals: 1/f noise (knee frequency 1Hz), Thermal noise, and "zero" noise, for the BB and EE polarization. Furthermore, figure 3.8 shows the residual maps obtained for the thermal noise, when the elevation for intensity and polarization Q-U maps is: 40°, 60°, and 80°.

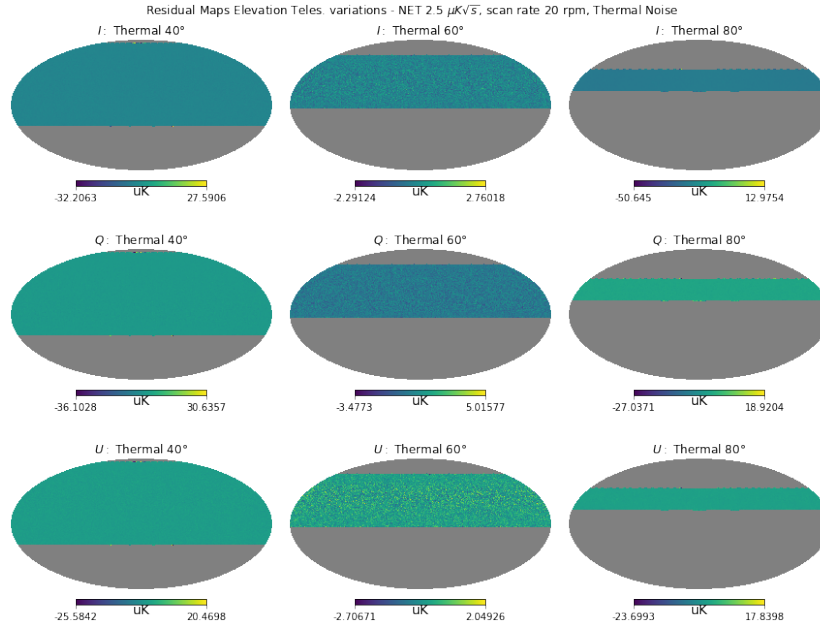


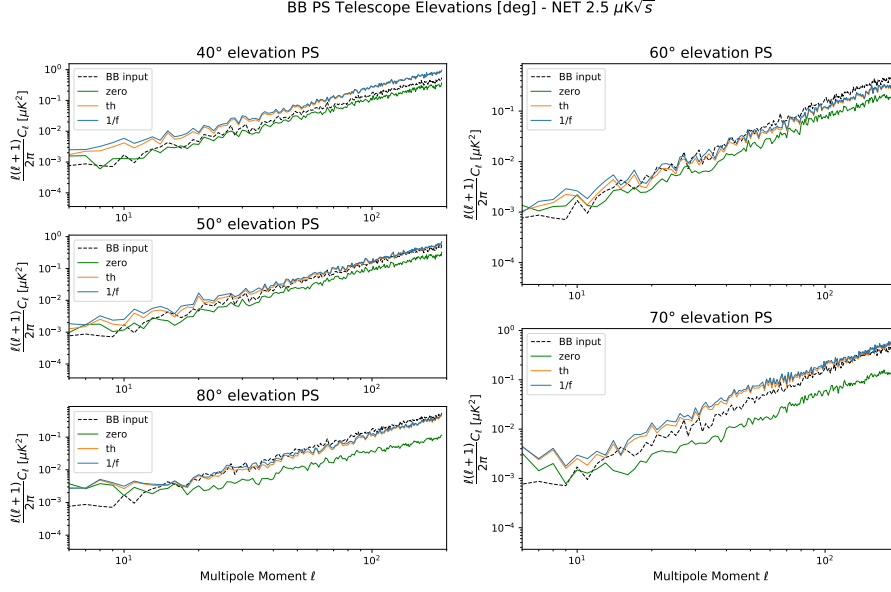
Figure 3.8.: The figure shows the residuals of the destriped maps when the telescope have thermal noise at elevation: 40°, 60°, and 80°.

Discussion

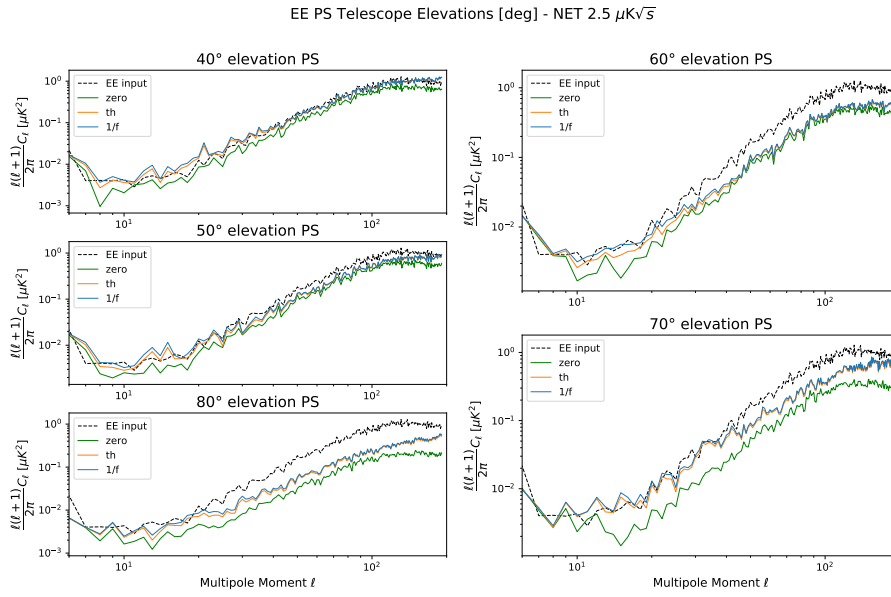
Figure 3.9 (a) shows the power spectrum of the BB mode signal. It is seen that the low elevation generates high amplitudes in the power spectrum at low multipoles, causing the output signal to deviate from the input signal. Also, we see that the 80° elevation appears to correctly follow the input signal when the multipole is $\ell > 11$; but when the multipole is between $6 < \ell < 11$, the output signal increases in amplitude (this also happens for the 70° elevation). Thus, it appears that the best elevation to observe the BB signal would be at 60°, even though the output signal does not exactly follow the input CMB signal. In the other hand, figure 3.9 (b), shows the power spectrum for the EE modes. Since this signal is higher than the BB mode signal, we observe that the best elevation to obtain this signal would be at 40°; however, when we observe the multipole between $6 < \ell < 11$, the signal seems more accurate at 60°. Finally, in figure 3.8 the residuals of the thermal maps are shown,

3. Results and Discussion

and although the observation at 40° will cover more sky than the other two elevations, the noise level is higher.



(a) Power Spectrum BB mode signal



(b) Power Spectrum EE mode signal

Figure 3.9.: The figure shows the polarization power spectrum PS for BB (a) and EE (b) modes when the telescope has elevations at $40^\circ, 50^\circ, 60^\circ, 70^\circ$, and 80° , compared with the PS of the input CMB map (in dashed line). NET $2.5 \mu\text{K}\sqrt{\text{s}}$, $1/f$ noise Knee frequency 1Hz, and scan rate 20 rpm.

3.7. Scan Rate Velocity

The scan strategy of the telescope consists of having a constant elevation and movement in the azimuth, so this scan movement is then circular. This scanning strategy, with this movement, is established because we could avoid $1/f$ noise effects when the telescope moves faster than the knee frequency of the $1/f$ noise. Figure 3.11 shows the behavior of the signal when the scan rate velocity of the telescope change from 0.33 rpm to 20 rpm.

The test simulates 5 different velocities 20 rpm ($120^\circ/s$), 3.33 rpm ($20^\circ/s$), 2.5 rpm ($15^\circ/s$), 1.66 rpm ($10^\circ/s$), and 0.33 rpm ($2^\circ/s$) to see the variations of the output signal. We simulates a $1/f$ signal noise with a knee frequency of 1Hz, and the telescope conditions are: elevation 60° , NET $2.5 \mu K\sqrt{s}$.

Discussion

Figure 3.11 shows that the signal with scan rate at 2 deg/s diverges from the input signal, while the signal at 120 deg/s tends to be closer to this signal. Therefore, even though these signals have a frequency of 1 Hz at the same elevation, the scan rate modified the output signal because the telescope is not able to avoid the effect of $1/f$ noise when the scan rate is lower than 120 deg/s . In the Temperature figure, there are no variations, but we can see big changes in the EE and BB figures. These changes show that when the scan rate goes to slower rotation speeds the telescope needs higher speeds to obtain the required low power signal.

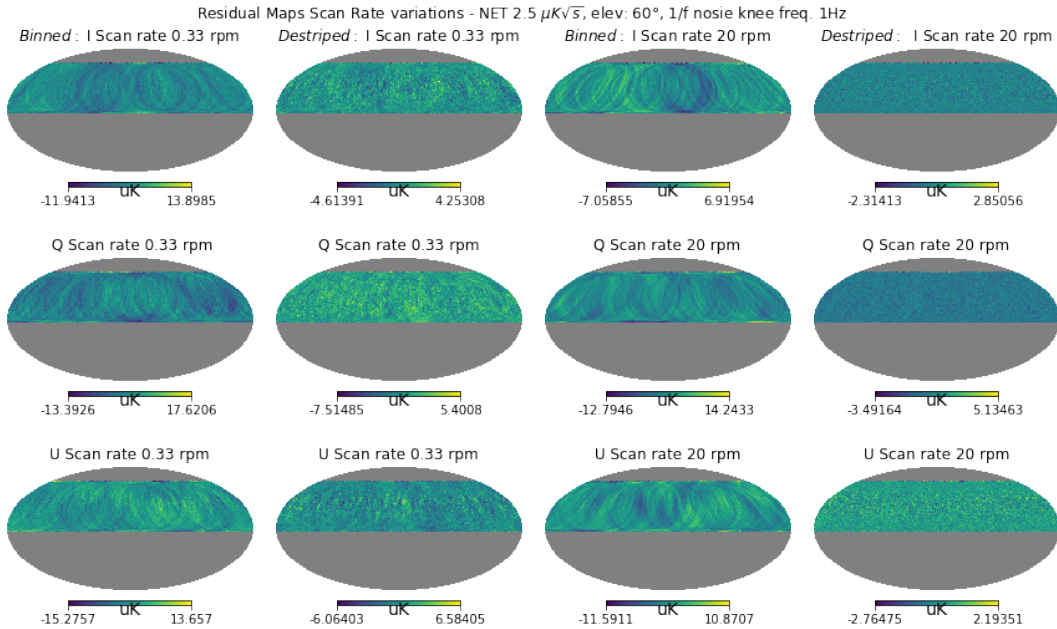


Figure 3.10.: The figure shows the residual maps of the binned and destriped maps when the telescope has a scan rate velocity of $2^\circ/s$ and $120^\circ/s$.

3. Results and Discussion

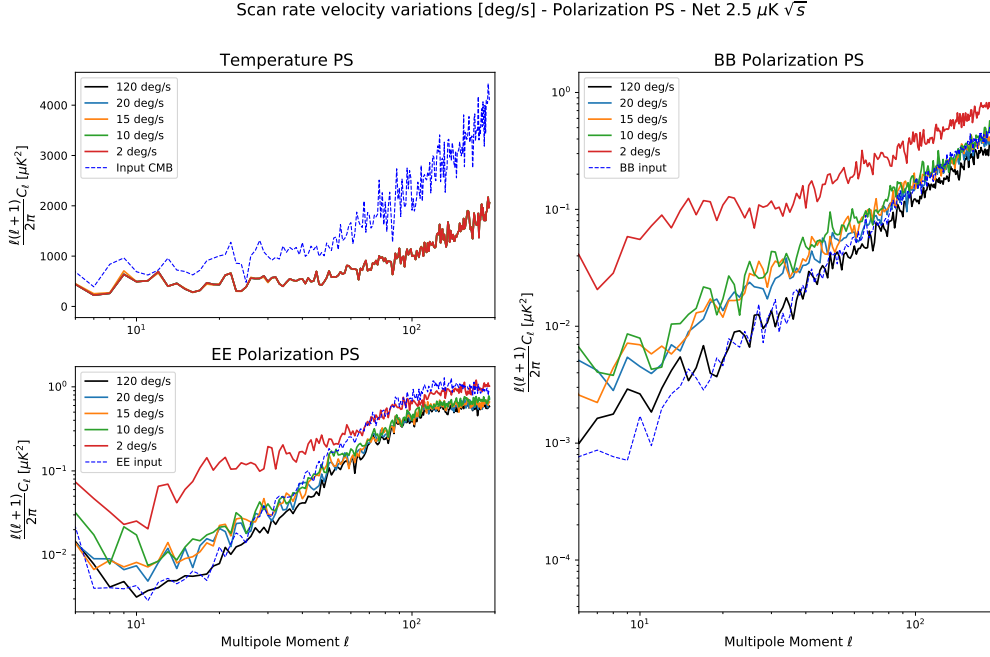


Figure 3.11.: The figure shows the polarization power spectrum PS for TT, EE and BB modes when the telescope have a scan rate velocity at $2^\circ/s$, $10^\circ/s$, $15^\circ/s$, $20^\circ/s$ and $120^\circ/s$ compared with the PS of the input CMB map (in dashed line). NET $2.5 \mu\text{K}\sqrt{s}$, $1/f$ noise Knee frequency 1Hz, and elevation 60° .

We can see that there is still a problem with the comparison between the output spectrum and the input spectrum. However, the main result is to see how the output changes at different rotations, and that as expected the telescope requires high scan rate speeds. On the other hand, figure 3.10 shows the residual maps for binned and destriped maps. We can see that when the scan rate is higher, the binned maps present less noise, and the result of the destriped map is improved.

4. Conclusions

In this project, a software code to simulate the GroundBIRD radio telescope was developed, using the TOAST software framework. The TOD object must have at least the following parameters to generate simulations: noise signal, weather file, latitude/longitude values of the place where the telescope is placed, simulation time, and the characteristics of the focal plane like geometric distribution of the detectors, polarization angles, NET value, Beam Size, and frequency sampling rate. All of these parameters are required to build a basic TOD object. Likewise, the input CMB model map determines the output signals of the simulation, and this input map and the TOD object create the pixel distribution map that will generate I, Q, and U maps.

The Map-Maker process created by the TOD object, the scanning strategy, and the signal noise generates a single *Binned map* that represents the entire simulation on one map. This binned map needs to be processed with a procedure called *Destriped* to remove correlated noise, and this process is provided by the *Libmadam* library which is included in the Map-Maker processing offering by the TOAST framework. Besides, it was shown that since the TOAST framework offers an open code, it can be adapted according to the needs of ground-based telescopes.

The simulation run-time requires at least 5 computer hours to simulate 24 hours of observation. Unnecessary functions need to be removed or improved. It is also possible to use the TOD object for one day to scale the response as the telescope observes the same sky every day. Therefore simulating years of observation takes months on the computer and that is not useful as we need to change several parameters and compare the results. Thus, reducing the $1/f$ noise would have required too much time and computational resources, which is not within the budgeted time to perform this project, since at least 1 week or 1 month of observation is needed to see the impact of this noise and estimate how much the $1/f$ noise smoothes out over time. Thus, an optimistic scenario was taken to test the $1/f$ noise, in which it was assumed that the $1/f$ noise is reduced as well as the thermal noise.

Since changing parameters is the ultimate objective of creating a virtual telescope, some important parameters were tested in this project. Firstly, the maps were affected by three noisy signals: thermal noise, $1/f$ noise, and a zero noise signal. This last "zero" signal is actually a very low thermal noise since the TOAST framework did not allow me to create a noiseless TOD object. Throughout the project, the results of these three signals are presented, and at a certain point, when telescope conditions improve, the thermal noise and zero noise closely match the input CMB signals.

As expected, some ringing patterns were observed in the binned maps where the $1/f$ noise signal is present. These patterns are observed due to the scanning strategy implemented in the telescope and the correlated noise that affects the TOD object. Consequently, these maps were manipulated with the map-maker module provided by the TOAST framework, and we obtained that the output destriped maps with correlated noise show much less noise compared to their binned map. Also, the binned thermal maps went through the *Libmadam* library and we observed that the binned and destriped maps are basically the same, and this occurs because the thermal noise has uncorrelated terms that cannot be avoided using the destriped library.

The integration time was improved and, as expected, the binned thermal noise map showed less noise. We tested 24 hours and three years of observation with a single detector and found that the thermal binned maps and $1/f$ noise present much less noise when running three years of observation. Likewise, we tested a scenario where the focal plane of the detectors has only two polarization angles, and another case in which it has four polarization angles, and the output polarization maps showed lower noise levels.

However, the long integration time and multiple polarization angles still present high noise levels. Hence, the output signals shown in the power spectrum are not close to the expected input signal. In this way, the calculation was made to obtain the NET value for three years when the number of detectors is 138. It was obtained that the NET value (if the observation efficiency is about 70 %) is equal to $2.5 \mu K \sqrt{s}$. Output maps with a NET value of $2.5 \mu K \sqrt{s}$ reduce the noise pixel level 10 times compared to the NET value of $24.7 \mu K \sqrt{s}$ for the Q-U polarization maps and the intensity maps when thermal and $1/f$ noise are present.

Although $1/f$ noise is not accurately represented, it is possible to observe the effects of this type of signal in the simulations. $1/f$ noise is a type of noise that depends on frequency, so the knee frequency value was tested when the NET value is $24.7 \mu K \sqrt{s}$ and $2.5 \mu K \sqrt{s}$. In both cases, it was obtained that the power spectrum signal decreases the amplitude when the knee frequency decreases, and it is the same behavior for the BB and EE signals. Furthermore, when the NET value is equal to $2.5 \mu K \sqrt{s}$, the BB signal is sloped, and the EE signal is curved. In both cases, the signal starts to be similar in amplitude to the input CMB signal as the knee frequency decreases. This means that decreasing the frequency of the $1/f$ noise makes it possible to detect large-scale signals from ground-based telescopes.

A relevant feature in the simulation is the elevation of the telescope since it determines the amount of sky that we will measure. It was shown that even when the elevation is 40° (so that the sky coverage is high), the noise level is higher than at elevations of 80° and 60° . This is because the amount of atmosphere the light has to pass through is dense, then the output data will be noisy. On the other hand, the 80° elevation has less sky coverage than the other two elevations, so the data is not sufficient for high-resolution mapping. Therefore,

60° elevation becomes the optimum degree of elevation to observe. Furthermore, the power spectrum shows that at an elevation $\ell < 11$ at 60° the output signal tends to respond better to the input signal than the other elevations.

Finally, once the previous conditions have been determined, one of the most relevant features of GroundBIRD, the scanning strategy, has been tested. The telescope must have a scan rate velocity that improves the effect of $1/f$ noise on the results. A $1/f$ noise signal with a knee frequency of 1 Hz was tested on the maps and the scan strategy velocity was changed. The results show that even when the signal has a low knee frequency value, if the scan frequency is lower, the output signal deviates from the input CMB signal, also it was shown that the binned output map has less noise when the scan rate is higher. It means that if the scan strategy were to improve the scan rate, the output signal would tend to be closer to the expected input CMB signal because the noise level at higher scan rates is lower. However, the simulation shown that even at 20 rpm the output signal at very low multipoles continues separate.

Thus, I consider that as future work this code could be improved since the TOAST framework has more modules to explore. For instance: modules to generate signals that simulate atmospheric noise or synchronous signals of the ground. Also, to have more realistic simulations, background effects generated by thermal dust and synchronous signals must be taken into account within the TOD object. In addition, the destriper process is available for testing in order to improve the results on the noise levels generated by the correlated signals. Improving the simulation would help to validate the primordial BB modes of polarization taking into account the characteristics of the GroundBIRD telescope, so that improvements in instrumentation and observing strategies can be critically implemented based on virtual telescope results.

A. Appendix

In this section we are going to add some extra information which will help to understand some concepts.

A.1. Simulations: *TOAST Classes*

The table A.2 shows the classes used in the simulation to generate the destripped maps. The table contains the name of the class and a description.

Class	Description
toast.mpi.Comm(mpiworld)	When passing the data through a toast workflow, the data is divided up among processes based on the details of the toast.Comm class that is used and also the shape of the process grid in each observation.
toast.tod.TOD()	This class is an example which provies the interface required to build the derivated classes.The base class provides detector pointing and timestreams for a single observation. Inside this class is calculated the pressure at the observer elevation, the scan strategy unique for the telescope, quaternions calculation for the elevation and azimuth and calculations to handle with the sample time of the detector
data = toast.Data(comm)	The data used by a TOAST workflow consists of a list of observations, and is encapsulated by the toast.Data class. A Data object contains a list of observations assigned to each process group in the Comm.
toast.tod.OpCacheClear().exec()	A Cache class behaves like a dictionary of N-dimensional numpy arrays. This class is used to ensure that when we clean simulated signals they really are delete of the memory.

Table A.1.: TOAST classes used to create the code base for simulations of GroundBIRD

Class	Description
toast.todmap.OpPointingHpix()	Each experiment might create other specialized pointing matrices used in solving for instrument-specific signals. This class help us to create the base for the sky signal model, simulate the atmosphere and the Scan Synchronous Signal of each detector.
toast.tod.OpSimNoise()	TOAST includes an operator that simulates basic sources. detector noise (1/f spectrum plus white noise), and also supports generating correlated noise by specifying a mixing matrix to combine individual detector streams with common mode. Operator which generates noise timestreams.
toast.todmap.OpSimAtmosphere()	For each observation, a realization of the physical atmosphere slab is created and moved according to the wind speed. Every detector sample is formed by a line of sight integral through this slab. This sort of real-space modelling naturally leads to correlated signal in the time domain that depends on atmospheric parameters and focalplane geometry.
toast.map.DistPixels()	Pixel domain data is distributed across an MPI communicator. Each process has a local data stored in one or more "submaps".
toast.todmap.OpSimScan()	Operator which generates sky signal by scanning from a map.The signal to use should already be in a distributed pixel structure,and local pointing should already exist.

Table A.2.: TOAST classes used to create the code base for simulations of GroundBIRD

Class	Description
toast.todmap.OpMapMaker()	In terms of algorithms built in to TOAST, there are 2 primary tools. The first is a wrapper around the external libmadam destripping map-maker. The second is a set of native mapmaking tools which are already quite usable for many common cases.
toast.todmap.SynchronousSignal()	Any systematic contaminant that is constant (for an observation) in the scanning reference frame (as opposed to sky coordinates), can be simulated as "Scan Synchronous Signal".

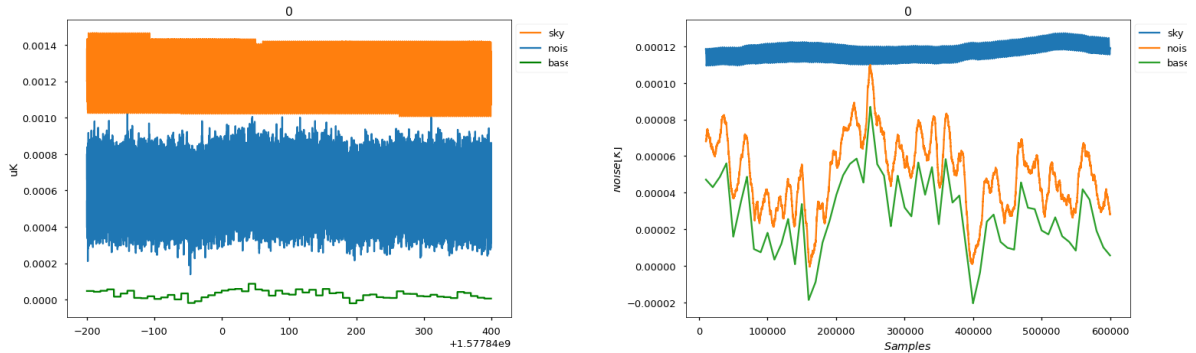
Table A.2.: TOAST classes used to create the code base for simulations of GroundBIRD

A.2. Module B

Hubble parameter	H_0	67.36
Total matter density	Ω_m	0.3153
Baryon density	$\Omega_b h^2$	0.022383
Cosmological constant	Ω_Λ	0.6847
Tensor to scalar ratio	r	0.00
Ionization optical depth	τ	0.0543

Table A.3.: Cosmological parameters of the input CMB Power Spectrum.

A.3. Module C



(a) Figure of the Time-stream result of ten minutes of simulation.

(b) Time-streams plot using the library `pandas.DataFrame.rolling` (window parameter 10000)

Figure A.2.: Time streams generated by the signals which affects the final maps to generate the binned map.

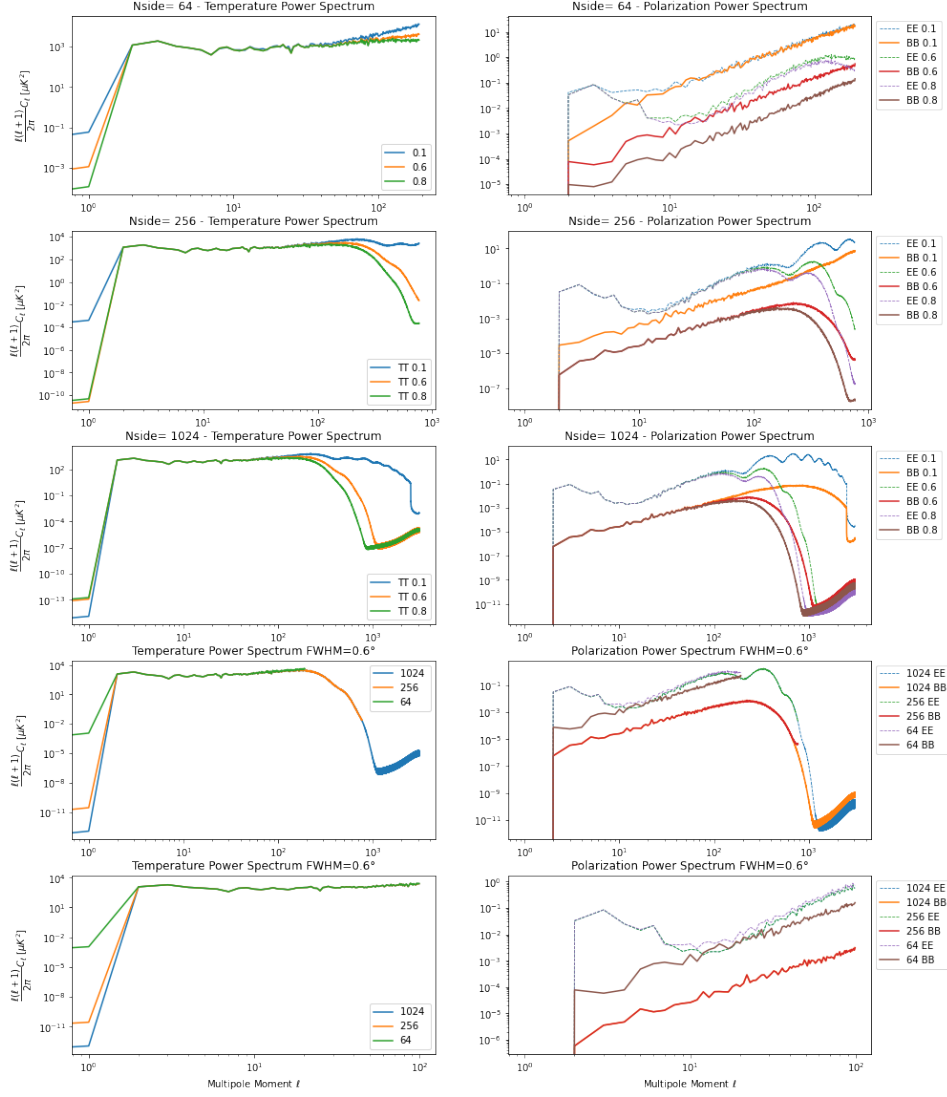


Figure A.1.: The figure shows the power spectrum PS result for temperature (at the right), and polarization EE and BB modes (at the left) of the input CMB map with Nside 64 (row one), 256 (row two), and 1024 (row three) when the telescope beam has FWHM at 0.1°, 0.6°, and 0.8°. The row four shows the PS with FWHM at 0.6° for the three Nside and the row five at multipole $l < 20$

List of Figures

1.1.	The three panels show 10-square-degree patches of all-sky maps. Image credit: NASA/JPL-Caltech/ESA	2
1.2.	Figure (a) shows the Thomson scattering effect when radiation an a quadrupole anisotropy generates linear polarization taken from (Hu et al., 1997). Figure (b) shows the polarization modes patterns generated by anisotropies taken from (Perlov et al., 2017)	5
	(a). Linear Polarization	5
	(b). Polarization modes patterns	5
1.3.	Figure (a) shows GroundBIRD telescope in the Teide observatory. Tenerife, Spain. Figure (b) shows the polarization Power Spectrum (PS) of the anisotropies as a function of the multipole. The orange region shows the GroundBIRD observation region Kutsuma, 2021	6
	(a). GroundBIRD Telescope	6
	(b). Polarization Power Spectrum	6
1.4.	Left: the electronic design of each pixel in the focal plane. Right: shows the layout of the focal plane. It contains 7 modules and 23 pixels for each module (Lee et al., 2020)	8
1.5.	Spectral characteristics of foregrounds and CMB in polarization. Magenta band shows polarized synchrotron emission, and red band polarized the thermal dust emission. The widths of the synchrotron and thermal dust bands are defined by the largest and smallest sky coverages (Jones et al., 2018) updated version with Quijote and GroundBIRD	9
1.6.	Flowchart of the principal classes of the TOAST framework. Figure shows that TOAST is divided into "Data" and "Operators". Data is related to how TOAST manages different data (TOD object, cache, noise), and Operators are functionalities that use Data and generate some results.	10
2.1.	The figure shows a screenshot of the "TOP" command while a script is running. It is possible to observe data like CPU (Percentage of CPU used by the process), RES (RAM memory used by the process), MEM (The percentage of RAM used by the process, that is, the RES value expressed as a percentage), TIME (total time spent in minutes)	13
	(a). screenshot 1	13
	(b). screenshot 2	13
2.2.	Flowchart showing the modules required to run the code for the GroundBIRD telescope simulation. Module A: the TOD object creation, module B: pixel mask, module C: creation of sky signal according to TOD object and pixel mask, module D: Map-making process.	14
2.3.	Scan strategy hits maps for GroundBIRD telescope. Figure shows scan strategy when simulation has 24 hours, 5 hours, and 10 minutes of observation time.	15
2.4.	Total precipitable water vapor [mm] for Atacama file. Figure at the left shows the mean values of 12 months for 24 hours and, figure at the right shows the mean value of 24 hours for 12 months of PWV.	16

List of Figures

2.5.	Figure shows the spatial distribution or geometry of the 23 detectors in a module. Furthermore, the polarization angles of each detector are indicated with and arrow.	17
(a).	Focal Plane polarization angles $0^\circ, 45^\circ, 90^\circ, 135^\circ$	17
(b).	Focal Plane polarization angles $0^\circ, 90^\circ$	17
2.6.	Time-streams and PSD (Power Spectral Density) for $1/f$ noise at knee frequency 10 Hz, Thermal Noise, and "zero" noise.	19
(a).	Time-stream plot for $1/f$ noise	19
(b).	Time-stream plot for Thermal noise	19
(c).	Time-stream plot for "Zero" noise	19
(d).	Power Spectral Density	19
2.7.	Figure shows the CMB map chosen as input or model to feed the simulation. This CMB map contains the Intensity, and polarization Q-U maps.	20
3.1.	The figure shows the intensity Binned and Destriped maps for observation time of 24 hours (center to the left) and 3 years (center to the right), with NET $820\mu K\sqrt{s}$ and $24.7\mu K\sqrt{s}$ respectively. From top to the bottom, we find the simulation output maps of the "zero", thermal, and $1/f$ noise signals.	26
3.2.	This figure shows the residual maps obtained after subtraction from the destriped maps of the $1/f$ noise (left), thermal noise (center), and zero noise (right) of the input CMB model signals. At the top, we find the intensity maps, in the center the polarization Q maps, and at the bottom the U maps results.	27
(a).	Simulation for 24 hours of integration time	27
(b).	Simulation for 3 years of integration time	27
3.3.	The figure shows the amplitude and residual maps for the $1/f$ and thermal signals for an observation time of 3 years (NET $24.7\mu K\sqrt{s}$) with the focal plane which contains polarization angles $0^\circ, 45^\circ, 90^\circ, 135^\circ$. At the top, intensity maps, in the center the polarization Q maps, and at the bottom polarization U maps. Column one and three shows the amplitude maps, and column two and four show the subtractions.	28
3.4.	The figure shows the power spectrum PS results of the amplitude maps of figure 3.3 compared with the PS of the input CMB map (in dash-line).	29
3.5.	The figure shows the amplitude and residual maps. Figure (a) shows the maps for the $1/f$ and thermal noise NET $2.5\mu K\sqrt{s}$, and figure (b) shows the zero noise maps for NET $2.5\mu K\sqrt{s}$ and $24.7\mu K\sqrt{s}$. At the top intensity maps, in the center polarization Q maps, and at the bottom polarization U maps. Column one and three shows the amplitude maps, and column two and four show the subtractions.	31
(a).	Maps for $1/f$ and thermal noise NET $2.5\mu K\sqrt{s}$	31
(b).	Maps for zero noise NET $2.5\mu K\sqrt{s}$ and $24.7\mu K\sqrt{s}$	31
3.6.	The figure shows the Power Spectrum PS of figure 3.5 maps compared with the PS of the input CMB map (in-dash line).	32

List of Figures

3.7.	The figure shows the power spectrum PS results for TT, EE, and BB modes when the 1/f noise has a knee frequency of 0.001 Hz, 0.1 Hz, 1 Hz, 10 Hz, 50 Hz, and 100 Hz compared with the PS of the input CMB map (in-dash line). Telescope elevation of 60° and scan rate 20 rpm . . .	33
(a).	Power Spectrum for NET equal to 24.8 $\mu\text{K}\sqrt{\text{s}}$	33
(b).	Power Spectrum for NET equal to 2.5 $\mu\text{K}\sqrt{\text{s}}$	33
3.8.	The figure shows the residuals of the destriped maps when the telescope have thermal noise at elevation: 40°, 60°, and 80°.	34
3.9.	The figure shows the polarization power spectrum PS for BB (a) and EE (b) modes when the telescope has elevations at 40°,50°,60°,70°, and 80°, compared with the PS of the input CMB map (in dashed line). NET 2.5 $\mu\text{K}\sqrt{\text{s}}$, 1/f noise Knee frequency 1Hz, and scan rate 20 rpm.	35
(a).	Power Spectrum BB mode signal	35
(b).	Power Spectrum EE mode signal	35
3.10.	The figure shows the residual maps of the binned and destriped maps when the telescope has a scan rate velocity of 2 °/s and 120 °/s.	36
3.11.	The figure shows the polarization power spectrum PS for TT, EE and BB modes when the telescope have a scan rate velocity at 2 °/s,10 °/s,15 °/s,20 °/s and 120 °/s compared with the PS of the input CMB map (in dashed line). NET 2.5 $\mu\text{K}\sqrt{\text{s}}$, 1/f noise Knee frequency 1Hz, and elevation 60°.	37
A.2.	Time streams generated by the signals which affects the final maps to generate the binned map.	43
(a).	Figure of the Time-stream result of ten minutes of simulation.	43
(b).	Time-streams plot using the library <i>pandas.DataFrame.rolling</i> (window parameter 10000)	43
A.1.	The figure shows the power spectrum PS result for temperature (at the right), and polarization EE and BB modes (at the left) of the input CMB map with Nside 64 (row one),256 (row two), and 1024 (row three) when the telescope beam has FWHM at 0.1°, 0.6°, and 0.8°. The row four shows the PS with FWHM at 0.6° for the three Nside and the row five at multipole $\ell < 20$. . .	44

List of Tables

1.1.	GroundBIRD telescope principal specifications taken from Choi, 2015	7
1.2.	The table shows calculations for the two principal observation frequencies. The telescope will observe half of the full-sky, for 3 years, with an efficiency of 70%. Also, the NET (Noise Equivalent of Temperature) was calculated following restrictions of the atmosphere and the detectors Lee et al., 2021	8
2.1.	Input parameters of the GroundBIRD simulation.	15
2.2.	The tables show the principal signals which will affect the simulated maps with their characteristics, also shows some values required to construct the pixel distribution map like NNZ (values per pixel), and Nside (resolution of the grid) (Gorski et al., 2005).	19
A.1.	TOAST classes used to create the code base for simulations of GroundBIRD	41
A.2.	TOAST classes used to create the code base for simulations of GroundBIRD	42
A.2.	TOAST classes used to create the code base for simulations of GroundBIRD	42
A.3.	Cosmological parameters of the input CMB Power Spectrum.	43

Bibliography

- Carroll, B. W., & Ostlie, D. A. (2014). *An introduction to modern astrophysics* (2nd ed.). Pearson New International Edition.
- Schneider, P. (2015). *Extragalactic astronomy and cosmology* (2nd ed.). Springer.
- Perlov, D., & Vilenkin, A. (2017). *Cosmology for the curious* (2nd ed.). Springer.
- Penzias, A. A., & Wilson, R. W. (1965). A Measurement of Excess Antenna Temperature at 4080 Mc/s., *142*, 419–421. <https://doi.org/10.1086/148307>
- KRAGH, H. S. (2007). *Conceptions of cosmos* (1st ed.). OXFORD.
- Peacock, J. A. (2010). *Cosmological physics* (1st ed.). CAMBRIDGE.
- Ade, P. A. R., Aghanim, N., Arnaud, M., Ashdown, M., Aumont, J., Baccigalupi, C., Banday, A. J., Barreiro, R. B., Bartlett, J. G., Bartolo, N., Battaner, E., Benabed, K., Benoit, A., Benoit-Lévy, A., Bernard, J.-P., Bersanelli, M., Bielewicz, P., Bock, J. J., Bonaldi, A., ... Zonca, A. (2016). Iplanck/i2015 results. *Astronomy & Astrophysics*, *594*, A12. <https://doi.org/10.1051/0004-6361/201527103>
- Ransom, J. J. C. S. M. (2016). *Essential radio astronomy* (1st ed.). Princeton University Press.
- Cepa, J. (2007). *Cosmología física* (1st ed.). Akal.
- Aghanim, N., Majumdar, S., & Silk, J. (2008). Secondary anisotropies of the CMB. *Reports on Progress in Physics*, *71*(6), 066902. <https://doi.org/10.1088/0034-4885/71/6/066902>
- Choi, J. (2015). *Groundbird: A telescope for the cosmic microwave background polarization measurement* (Doctoral dissertation). Korea University.
- Hu, W. (2003). CMB temperature and polarization anisotropy fundamentals. *Annals of Physics*, *303*(1), 203–225. [https://doi.org/10.1016/s0003-4916\(02\)00022-2](https://doi.org/10.1016/s0003-4916(02)00022-2)
- Hu, W., & White, M. (1997). A CMB polarization primer. *New Astronomy*, *2*(4), 323–344. [https://doi.org/10.1016/s1384-1076\(97\)00022-5](https://doi.org/10.1016/s1384-1076(97)00022-5)
- Ade, P. A. R., Ahmed, Z., Amiri, M., Barkats, D., Thakur, R. B., Bischoff, C. A., Beck, D., Bock, J. J., Boenish, H., Bullock, E., Buza, V., Cheshire, J. R., Connors, J., Cornelison, J., Crumrine, M., Cukierman, A., Denison, E. V., Dierickx, M., Duband, L., ... Zhang, S. (2021). Improved constraints on primordial gravitational waves using planck, wmap, and bicep/keck observations through the 2018 observing season. *Phys. Rev. Lett.*, *127*, 151301. <https://doi.org/10.1103/PhysRevLett.127.151301>
- Kutsuma, H. (2021). *Development of novel calibration methods and performance forecaster of cutting-edge superconducting detector mkids for cmb experiments* (Doctoral dissertation). Astro-nomical Institute, Graduate School of Science, Tohoku University.
- Honda, S., Choi, J., Génova-Santos, R. T., Hattori, M., Hazumi, M., Ikemitsu, T., Ishida, H., Ishitsuka, H., Jo, Y., Karatsu, K., Kiuchi, K., Komine, J., Koyano, R., Kutsuma, H., Lee, K., Mima, S., Minowa, M., Moon, J., Nagai, M., ... Yoshida, M. (2020). On-site performance of GroundBIRD, a CMB polarization telescope for large angular scale

- observations. In H. K. Marshall, J. Spyromilio, & T. Usuda (Eds.), *Ground-based and airborne telescopes VIII* (pp. 1379–1386). SPIE. <https://doi.org/10.1117/12.2560918>
- Lee, K., Choi, J., Génova-Santos, R. T., Hattori, M., Hazumi, M., Honda, S., Ikemitsu, T., Ishida, H., Ishitsuka, H., Jo, Y., Karatsu, K., Kiuchi, K., Komine, J., Koyano, R., Kutsuma, H., Mima, S., Minowa, M., Moon, J., Nagai, M., . . . Yoshida, M. (2020). Groundbird: A cmb polarization experiment with mkid arrays. *Journal of Low Temperature Physics*, 200(5–6), 384–391. <https://doi.org/10.1007/s10909-020-02511-5>
- Kitchin, C. (2013). *Astrophysical techniques (6th ed.)* (6th ed.). CRC Press.
- Lee, K., Génova-Santos, R. T., Hazumi, M., Honda, S., Kutsuma, H., Oguri, S., Otani, C., Peel, M. W., Sueno, Y., Suzuki, J., Tajima, O., & Won, E. (2021). A forecast of the sensitivity on the measurement of the optical depth to reionization with the groundbird experiment. *The Astrophysical Journal*, 915(2), 88. <https://doi.org/10.3847/1538-4357/ac024b>
- Lee, K., Choi, J., Génova-Santos, R. T., Hattori, M., Hazumi, M., Honda, S., Ikemitsu, T., Ishida, H., Ishitsuka, H., Jo, Y., Karatsu, K., Kiuchi, K., Komine, J., Koyano, R., Kutsuma, H., Mima, S., Minowa, M., Moon, J., Nagai, M., . . . Yoshida, M. (2020). GroundBIRD: A CMB polarization experiment with MKID arrays. *Journal of Low Temperature Physics*, 200(5–6), 384–391. <https://doi.org/10.1007/s10909-020-02511-5>
- Jones, M. E., Taylor, A. C., Aich, M., Copley, C. J., Chiang, H. C., Davis, R. J., Dickinson, C., Grumitt, R. D. P., Hafez, Y., Heilgendorff, H. M., Holler, C. M., Irfan, M. O., Jew, L. R. P., John, J. J., Jonas, J., King, O. G., Leahy, J. P., Leech, J., Leitch, E. M., . . . Zuntz, J. (2018). The c-band all-sky survey (c-BASS): Design and capabilities. *Monthly Notices of the Royal Astronomical Society*, 480(3), 3224–3242. <https://doi.org/10.1093/mnras/sty1956>
- Guidi, F., Rubiño-Martín, J. A., Pelaez-Santos, A. E., Génova-Santos, R. T., Ashdown, M., Barreiro, R. B., Bilbao-Ahedo, J. D., Harper, S. E., & Watson, R. A. (2021). The scppicasso/scp map-making code: Application to a simulation of the QUIJOTE northern sky survey. *Monthly Notices of the Royal Astronomical Society*, 507(3), 3707–3725. <https://doi.org/10.1093/mnras/stab2422>
- Kurki-Suonio, H., Keihänen, E., Keskitalo, R., Poutanen, T., Sirviö, A.-S., Maino, D., & Burigana, C. (2009). Destriping CMB temperature and polarization maps. *Astronomy & Astrophysics*, 506(3), 1511–1539. <https://doi.org/10.1051/0004-6361/200912361>
- Górski, K. M., Hivon, E., Banday, A. J., Wandelt, B. D., Hansen, F. K., Reinecke, M., & Bartelmann, M. (2005). HEALPix: A Framework for High-Resolution Discretization and Fast Analysis of Data Distributed on the Sphere., 622, 759–771. <https://doi.org/10.1086/427976>
- Zonca, A., Singer, L., Lenz, D., Reinecke, M., Rosset, C., Hivon, E., & Gorski, K. (2019). Healpy: Equal area pixelization and spherical harmonics transforms for data on the sphere in python. *Journal of Open Source Software*, 4(35), 1298. <https://doi.org/10.21105/joss.01298>
- Castro-Almazán, J., Muñoz-Tunon, C., Lorenzo, B., Perez Jordan, G., Varela, A., & Romero, I. (2016). Precipitable water vapour at the canarian observatories (teide and roque de los muchachos) from routine gps, 99100P. <https://doi.org/10.1117/12.2232646>

- Lorenzo, B., Castro-Almazán, J., eff-darwich, A., Munoz-Tunon, C., Pinilla-Alonso, N., Rodriguez Espinosa, J., & Romero, I. (2009). Precipitable water vapour content above the roque de los muchachos observatory from gps estimations. *Proceedings of SPIE - The International Society for Optical Engineering*, 7475. <https://doi.org/10.1117/12.830235>
- Bustos, R., Rubio, M., Otarola, A., & Nagar, N. (2014). Parque astronomic de atacama: An ideal site for millimeter, submillimeter, and mid-infrared astronomy. *Publications of the Astronomical Society of the Pacific*, 126. <https://doi.org/10.1086/679330>
- Poletti, D., Fabbian, G., Jeune, M. L., Peloton, J., Arnold, K., Baccigalupi, C., Barron, D., Beckman, S., Borrill, J., Chapman, S., Chinone, Y., Cukierman, A., Ducout, A., Elleflot, T., Errard, J., Feeney, S., Goeckner-Wald, N., Groh, J., Hall, G., ... Whitehorn, N. (2017). Making maps of cosmic microwave background polarization for ib/i-mode studies: The POLARBEAR example. *Astronomy & Astrophysics*, 600, A60. <https://doi.org/10.1051/0004-6361/201629467>
- Liccardo, V., de Mericia, E. J., Wuensche, C. A., Abdalla, E., Abdalla, F. B., Barosi, L., Brito, F. A., Queiroz, A., Villela, T., Peel, M. W., Wang, B., Costa, A. A., Ferreira, E. G. M., Fornazier, K. S. F., Novaes, C. P., Santos, L., dos Santos, M. V., & et al. (2021). The BINGO project. IV. simulations for mission performance assessment and preliminary component separation steps. *Astronomy & Astrophysics*. <https://doi.org/10.1051/0004-6361/202140886>
- Sutton, D., Johnson, B. R., Brown, M. L., Cabella, P., Ferreira, P. G., & Smith, K. M. (2009). Map making in small field modulated CMB polarization experiments: Approximating the maximum likelihood method. *Monthly Notices of the Royal Astronomical Society*, 393(3), 894–910. <https://doi.org/10.1111/j.1365-2966.2008.14195.x>
- Delabrouille, J. (1998). Analysis of the accuracy of a destriping method for future cosmic microwave background mapping with the planck surveyor satellite. *Astron. Astrophys. Suppl. Ser.*, 127(3), 555–567. <https://doi.org/10.1051/aas:1998119>
- Gorski, K. M., Hivon, E., Banday, A. J., Wandelt, B. D., Hansen, F. K., Reinecke, M., & Bartelmann, M. (2005). HEALPix: A framework for high-resolution discretization and fast analysis of data distributed on the sphere. *The Astrophysical Journal*, 622(2), 759–771. <https://doi.org/10.1086/427976>
- Keihänen, E., Keskitalo, R., Kurki-Suonio, H., Poutanen, T., & Sirviö, A.-S. (2010). Making cosmic microwave background temperature and polarization maps with MADAM. *Astronomy and Astrophysics*, 510, A57. <https://doi.org/10.1051/0004-6361/200912813>